EÖTVÖS LORÁND UNIVERSITY

FACULTY OF INFORMATICS

INSTITUTE OF CARTOGRAPHY AND GEOINFORMATICS

Comparison of the Effect of Atmospheric Correction Methods on Chlorophyll-a Estimation in Fúquene Lagoon

Sara Alejandra Mendoza Urrea

student of Cartography MSc

András Jung

Associate Professor

ELTE Institute of Cartography and Geoinformatics

Budapest, 2021

EÖTVÖS LORÁND UNIVERSITY
FACULTY OF INFORMATICS
Department of Cartogrphy and Geoinformatics

Thesis Registration Form

Student's Data:
   Student's Name: Mendoza Urrea Sara Alejandra
   Student's Neptun code: D07ENT

Course Data:
   Student's Major: Cartography MSc

I have an internal supervisor

Internal Supervisor's Name: *Jung András*
   Supervisor's Home Institution: *ELTE IK Institute of Map Science and Geoinformatic*
   Address of Supervisor's Home Institution: *Budapest, Pázmány Péter stny. 1/A, 1117. Room: 7/82.*
   Supervisor's Position and Degree: *Habilitated Associated Professor*

Thesis Title: Estimation for the seasonal change of the trophic state of Lake Lupa Beach, in Hungary, by remote sensing.

Topic of the Thesis:
(Upon consulting with your supervisor, give a 150-300-word-long synopsis os your planned thesis.)

Investigate the possibility to define the changes in the water quality of artificial lake Lupa Beach, through the use of satellite images (using open sources as Landsat, and Sentinel images). And, explore the possible quantitative and/or qualitative seasonal changes, in the aim to construct a model that relates a possible eutrophication throughout the year with the recreational activities conducted there.

The artificial lake Lupa Beach, serves as an immediate tourist destination for the people living on the central region of Hungary. On summer season, the lake receives a considerable amount of people, which has created an impact regarding the natural trophic state of the water. Not only on a superficial level, but possibly on a groundwater level, which could bring some consequences to the near aquifers and so to the near population of Budakalász.

Budapest, 2020.11.29.

TABLE OF CONTENTS

LIST OF FIGURES

LIST OF TABLES

ABSTRACT

The importance of freshwater lakes and reservoirs in ecosystem services leads to the high need for monitoring lake water quality both at local and global scales. The study aimed to see the effect of different atmospheric correcting methods in the potential suitability of Sentinel-2 Multispectral Imager (MSI) sensor, and Landsat 8 Operational Land Imager (OLI) sensor data from years 2015 to 2021, for mapping chlorophyll a (Chl-a) concentration in Fúquene Lagoon, one of the most important and heavily eutrophicated freshwater bodies in Colombian Andes. The methodology followed an atmospheric correction stage where Sen2cor atmospheric correction software was used for Sentinel-2 imagery with the Atmospheric Precorrected Differential Absorption (APDA) algorithm, while Landsat 8 imagery datasets were downloaded in an atmospherically corrected format, with Land Surface Reflectance Code (LaSRC) algorithm. Chl-a concentration was estimated with a band ratio established reflectance algorithm derived from the Normalized Chlorophyll Index (NDCI). Results present the Chl-a distribution maps over time, showing a spatial dynamic of the parameter in the lagoon, for both satellites. The comparison between the results from the atmospheric correction methods in both satellites showed most of the time an overestimation of the Chl-a concentration for Sentinel-2 images corrected with the APDA method. In situ measurements were not available; therefore, it was not possible to validate the quantitative performance of the Chl-a concentration algorithm, therefore further validation in tropical water bodies is expected to complete the research.

INTRODUCTION

Continental freshwaters, also known as inland waters, are a fundamental global resource, that fulfills several important functions, as being key to the biodiversity of a region, be part of the global biochemical cycles, and serve as the core to food and energy production to human development. (Tyler et al., 2016).

Furthermore, as changing environment sentinels, inland water bodies must be monitored to provide guidelines for their exploitation, appropriate use, and most important for their preservation. However, due to their uneven global distribution and extension, since their sizes vary from small (i.e., ponds) to large (i.e., Great Lakes) (D. R. Mishra et al., 2017), and due to their geographic location that may be difficult to access, given the topography of a region; the traditional field-based methods with in-situ data to monitor the water quality had been changing rapidly for the use of remote sensing techniques.

Remote sensing technology uses sensor systems that record the interaction between the electromagnetic energy or radiation emitted by a source and reflected by a target, which provides information on the optical properties of such target. For aquatic environments, it has been used since the 1970s, developing concepts for hydrologic optics, known today as bio-optical modeling, to monitor optically active water constituents such as total suspended solids (TSS), color dissolved organic matter (CDOM), and chlorophyll-a (Chl-a) (Jerlov, 2014).

In the present work, a high Andean lagoon found in the tropical Andes was chosen to be the study case. The Fúquene Lagoon, located in Colombia, is the main component of the hydrographic system of the northern region of the Cundiboyacense highlands, and is one of the most important lagoon systems worldwide, as it is home to more than 164 species of birds, a biological corridor for migratory birds, and is home to endemic species, making it a priority ecosystem for biodiversity conservation. (CAR, 2021).

The Lagoon has been severely affected by anthropogenic actions; which has caused a disbalance in the ecosystem, increasing biomass production and accelerating a eutrophication process that degrades the quality of the water. To monitor this process, the trophic state can be assessed with the estimation of Chl-a concentration in the water, as it is an index of phytoplankton abundance and biomass production, and thus of the quality of the water in the lagoon.

Using imagery from Sentinel-2/MSI and Landsat 8/OLI satellites from the year 2015 to the year 2021 for the dry season of the study case area, the main objective for the present work was to see the effect of the atmospherical correction methods used in both satellites, as the atmospheric impacts on optical observations is a fundamental pre-analysis step for any quantitative analysis. Methods Dark Object Subtraction (DOS), Atmospheric Precorrected Differential Absorption (APDA), and Land Surface Reflectance Code (LaSRC); were compared in the performance of an empirical algorithm used to estimate Chl-a concentration, derived from the Normalized Difference Chlorophyll Index (NDCI), which is based on the Chl-a reflectance peak wavelength.

To achieve this, a qualitative and quantitative comparison was made between the thematic maps resulting from Chl-a concentration, where an absolute statistical comparison and an image classification quality comparison were carried out.

As an important note, despite it was not possible to perform a validation with real in situ data of Chl-a content from the lagoon; efforts to find an appropriate atmospheric correction method and algorithm, that works for the region and its special climate conditions, and provide accurate results for the optical water parameters, would highly improve the quality and efficiency of monitoring Fúquene lagoon ecosystem, and so, future investigations are expected to complete this research.

1. LITERATURE REVIEW AND CONCEPTUAL BACKGROUND

1.1. Remote Sensing

Remote sensing can be defined as the process of acquiring, processing, and interpreting images, and related data, that are normally obtained through aircrafts and satellites in a remote way, with sensor systems that record the interaction between **electromagnetic energy** reflected and emitted, and a target such as the surface of the Earth (Sabins & Ellis, 2020). This interaction can happen in form of visible light, heat, and microwaves, and it is determined by the physical properties of the matter, and the wavelength of electromagnetic energy sensed by the remote device.

There are several components involve in this process. As seen in Figure 1, the first requirement is the energy source, which can determine whether is a *passive remote sensing* process, where the sun is used as the source of electromagnetic energy and the sensors measure reflected solar radiation in visible, near-infrared, and mid-infrared wavelengths (Dong & Chen, 2017). Or, an *active remote sensing* process, where the sensor has its own source of energy that is directed towards the target or object, to get the measurement of the emitted energy back.
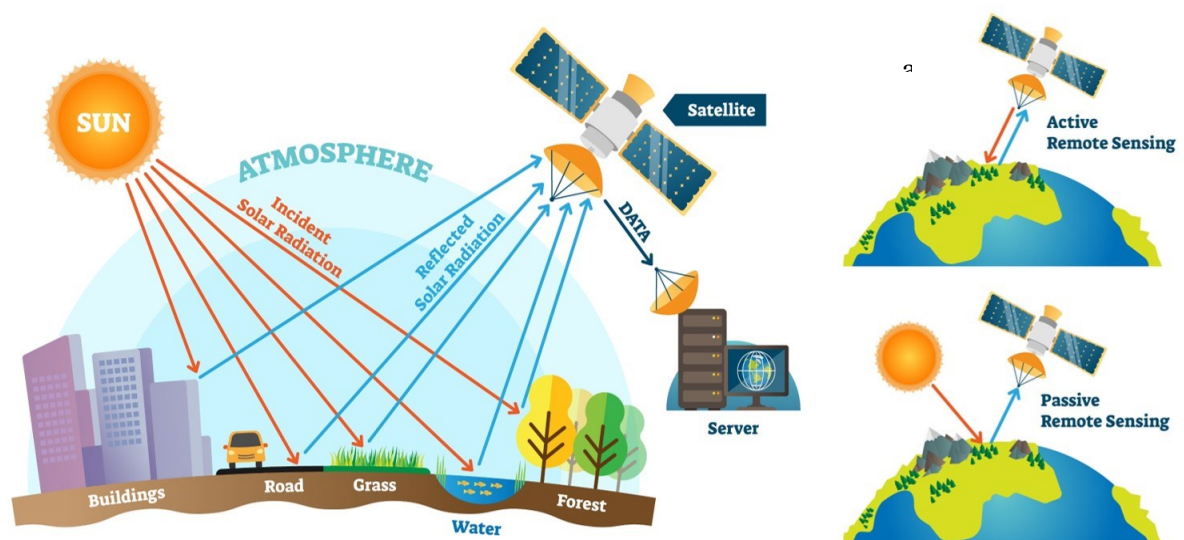
Figure 1. Remote sensing process, a) Depiction of active remote sensing; b) Depiction of passive remote sensing. Source: Taken from(VectorMine, n.d.)

The information collected by the sensors is transmitted to Earth as a digital signal, in a numeric matrix form. In the reception systems, *a priori* treatment of the image is made where some geometric or radiometric errors are debugged, before being distributed to users (Estruch, 2010).

Finally, the images in analog or digital format are analyzed by the users. These interpretations and treatments allow obtaining new information such as thematic maps and statistical data, etc.

During the interaction between ER and matter, illustrated in Figure 2, the incident radiation can be:

- Transmitted, when the energy passed through the substance.

- Absorbed, where the energy is given up mostly to heating the matter.

- Reflected, here the energy is returned unchanged with the angle of incidence equal to the angle of reflection. Reflectance is the ratio of reflected energy to that incident on a body. The wavelength reflected (not absorbed) determines the color of an object (Sabins & Ellis, 2020).

- Scattered, that is when the direction of the energy propagation is randomly changed. Normally atmospheric particles will cause this effect.

- Emitted, where the energy is first absorbed, then re-emitted, usually at longer wavelengths. The object heats up.
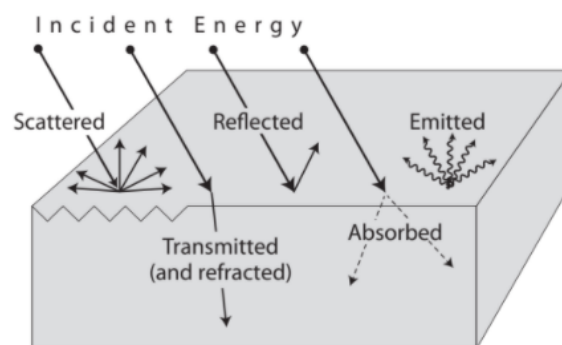
Figure 2. Interaction processes between ER and matter. Source: Taken from(Sabins & Ellis, 2020)

1.1.1. *Electromagnetic Radiation*

This electromagnetic radiation (ER), refers to the energy that moves with the velocity of light in a harmonic wave pattern; meaning that the waves occur at equal intervals in time. (Sabins & Ellis, 2020). This radiation consists of an electrical field (E) that varies in magnitude in a direction perpendicular to the direction of propagation. In addition to a magnetic field (H) oriented at right angles to the electrical field (Campbell & Wynne, 2011).

The behavior of these waves can be explained by their properties, as it is shown in Figure 3, where the wavelength (λ) of electromagnetic waves is the distance from any point on one cycle or wave, to the same position on the next cycle or wave. This will also give us the frequency (v), as the number of times a cycle is repeated in one second, and given that all ER travels at the same velocity, commonly known as the speed of light (denoted with the letter c, for practical purposes is equal to 3 x 10^8 m*sec$^{-1)}$, the mathematical relation between these three can be represented as follows,

$$c = v\lambda \quad or \quad \lambda = \frac{c}{v}$$

1] *[*

As equation [1] shows, the frequency of light is inversely proportional to its wavelength, such that the greater the wavelength, the smaller the frequency and vice versa.
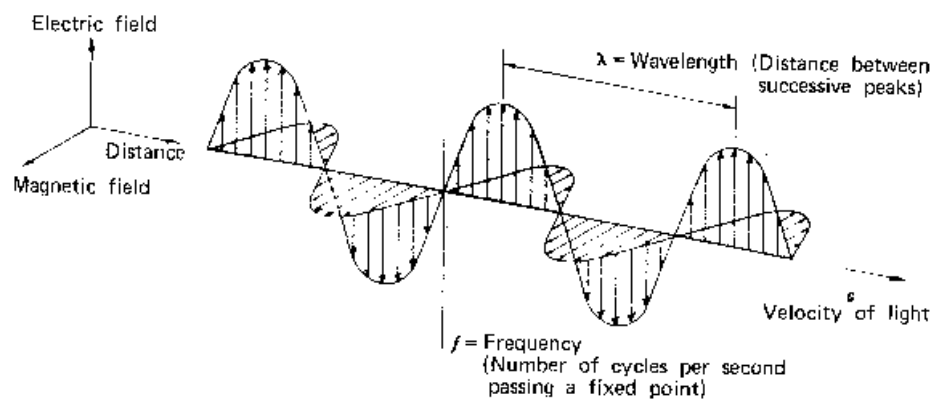
Figure 3. Components of the electromagnetic wave. Source: Taken from (Campbell & Wynne, 2011)

1.1.2. Electromagnetic Spectrum

As stated previously, each object or matter has its own wavelength range, which has been classified and located in function to the wavelength in the ***electromagnetic spectrum*** (Figure 4), which is a compendium of all the ranges of ER in spectral regions, from nanometers (gamma rays, x-rays) to meters (used in telecommunications as microwaves) of wavelengths, being the micrometer (μm) the designated unit for the ER (Sabins, 2007).
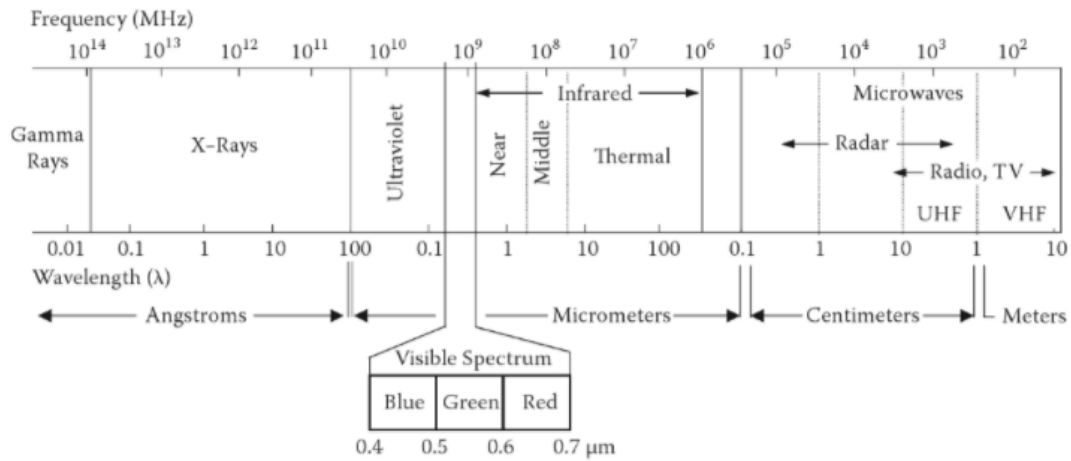
Figure 4. Electromagnetic Spectrum, showing the different regions classified by the wavelength. Source:(Chuvieco & Huete, 2009)

Currently, space sensors use a reduced field of wavelengths ranging from the visible spectrum (comprised between 0.4 and 0.7 µm), up to the microwave domain (waves of more than one millimeter), passing at an intermediate location, through the spectral regions of near, medium and thermal infrared, as shown on Table 1.

This however can be affected due to the action of certain chemical compounds located in the atmosphere, which cause an absorbing effect in specific regions of the spectrum, which limits the capture of radiation from the Earth (Estruch, 2010).

Table 1. Spectral regions and bands currently used in remote sensing, with their main characteristics.

Spectral regions and bands	Wavelength	Description
Visible Region (VIS)	0.4 to 0.7 µm	Is the spectral region that the human eye is capable of detecting, and can be divided into three primary colors, blue, red, and green.
• Blue band	0.4 to 0.5 µm	Scattered by the atmosphere. Absorbed by chlorophyll in plants.
• Green band	0.5 to 0.6 µm	Includes peak reflected energy on the Earth.
• Red band	0.6 to 0.7 µm	Absorbed by chlorophyll in plants.

Spectral regions and bands	Wavelength	Description
Infrared Region	0.7 to 1000 μm	This spectrum lies beyond human eye perception capability.
• Near-Infrared (NIR)	0.7 to 0.9 μm	Solar radiation is strongly reflected by green vegetation.
• Shortwave infrared (SWIR)	0.9 to 3.0 μm	It is commonly used in the identification of minerals, as well as estimating soil and vegetation moisture (Chuvieco & Huete, 2009).
• Thermal infrared (TIR)	3.0 to 5.0 μm	Useful for "hot" targets (e.g., fires or volcanoes). Also known as Medium wavelength IR (MWIR).
	8.0 to 14.0 μm	Useful for "warm" targets (e.g., land and oceans). Also known as Long wavelength IR (LWIR)
Microwave region	0.1 to 100 cm	This spectrum of very large wavelength is transparent to clod cover and enables us to "see" through clouds. They can also penetrate forest canopies to various depths
• Passive methods	0.1 to 100 cm	Used for soil moisture and surface roughness analyses.
• Active methods (radar)	0.8 to 100 cm	

Source: (Chuvieco & Huete, 2009; Sabins & Ellis, 2020)**.**

1.1.3. Radiance and reflectance

When using satellite imagery, there are two important concepts to keep in mind, radiance, which is the variable measured by the remote sensing instrument, which includes the radiation scattered by the atmosphere as well as the radiation reflected by the target. And the reflectance, which is the proportion of the radiation striking a surface to the radiation reflected off of it.

Figure 5 shows a simplified diagram of a passive remote sensing and how atmospheric scattering directs unwanted radiation (denominated path radiance) into the sensor, which is then combined with the target reflectance to form an unwanted total radiance measurement from the target of interest.
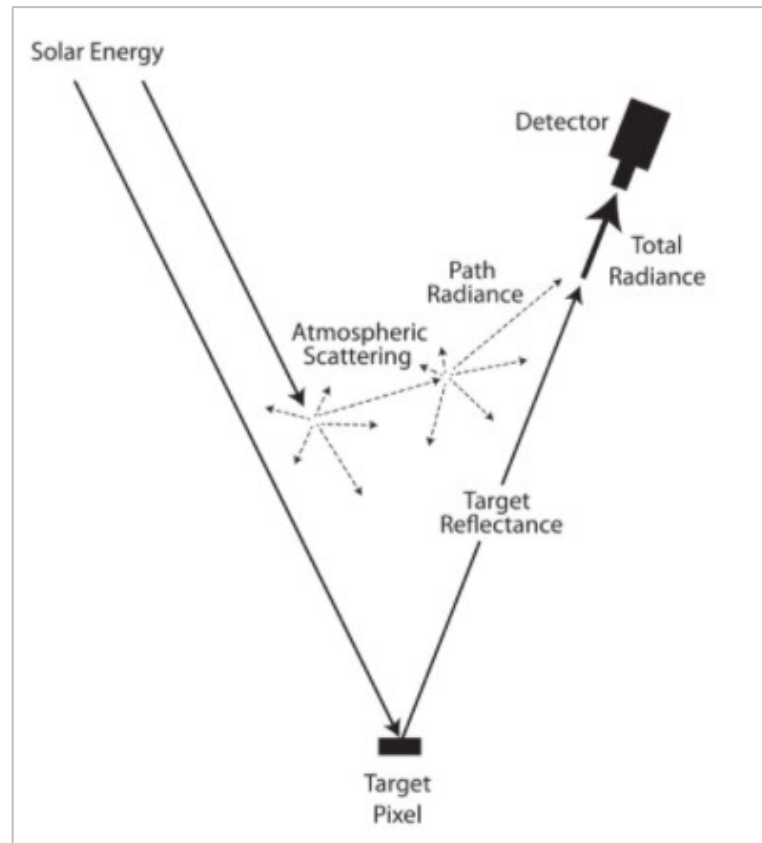
Figure 5. Simplified diagram showing radiance and reflectance processes. Source:(Sabins & Ellis, 2020)

To avoid this, satellite imagery is corrected atmospherically to obtain surface reflectance, which is a much more accurate value when using spectral bands to compute and estimate the physical characteristics of the Earth´s surface.

1.2. Remote sensing in inland water quality monitoring

Nowadays, one of the main interests of humankind is to regulate the exploitation, use, utilization, and preservation of the quality and quantity of water resources. This has motivated the development of new technologies that facilitate and improve the efficiency of techniques for water quality monitoring; and as opposed to the traditional field-based methods, which are usually costly and work-intensive, remote sensing offers a low-cost, high frequency, broad coverage, and practical alternative for water quality assessment and monitoring (Duan et al., 2010).

The use of remote sensing techniques in aquatic environments has been intensely developed during the 1960s with the beginning of the era of satellites, mainly for optical oceanography (D. R. Mishra et al., 2017), establishing, as a result, the concepts of hydrologic optics and radiative transfer, known today as bio-optical modeling . However, the application

of this theories and concepts, were applied to inland waters only during the last three decades to monitor optically active water constituents, such as chlorophyll-a, total suspended solids (TSS), color dissolved organic matter (CDOM), and others (Jerlov, 2014).

The slower process developed in inland waters has been attributed to the variability in the water constituents, that as (Morel & Prieur, 1977) proposed, generates a classification for water bodies: case 1 and case 2. The first one refers to deep blue waters where the reflectance ratio between the wavelengths 443 and 550 nm is bigger than 1.0. And case 2 waters, which are the common green waters, referred to as complex waters (Gitelson et al., 2008; Topp et al., 2020a), with higher turbidity and with the presence of dissolved and suspended matter that increases both, absorption and scattering, resulting in a reflectance radio smaller than 1.0. (D. R. Mishra et al., 2017). Such classification, although not always accurate, has been widely used by researchers as an easy way to categorize the types of water bodies used in remote sensing bio-optical modeling.

When talking about inland waters, the concept refers to aquatic environments typically confined within the land boundaries that provide exceptionally important ecological, environmental, hydrological, and socioeconomic services to mankind, given the fact that they serve as sentinels to changing environments (D. R. Mishra et al., 2017).

1.2.1. *Optical water properties and parameters:*

Remote sensing of inland water is based on the optical properties of the water, given by the interaction between the radiation and the target water body. These properties can be divided into two categories as apparent optical properties (AOP), which depend on the medium and the directional structure of the light or radiation, Figure 6 illustrates this configuration for a passive remote sensing process. And, inherent optical properties (IOP), which depend only on the medium. (Preisendorfer et al., 1976).
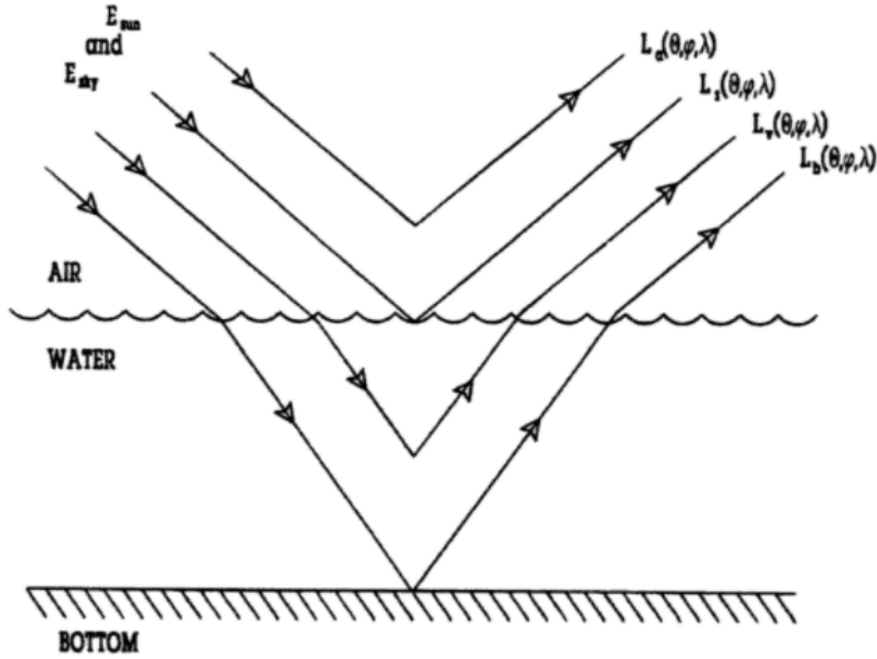
Figure 6. Components of the radiance recorded by a remote sensor over a natural water body. Source: Taken from (Bukata et al., 2018)

In Figure 6, where E_{sky} and E_{sun} are the skies and solar irradiances respectively, the depiction of the radiance recorded by the remote sensor, L_t ,can be represented by the expression *(1)*, which comprise the following components:

$$L_t = L_a + L_s + L_v + L_b \qquad\qquad (1)$$

L_a, which is the portion of the recorded radiance resulting from the radiation that does not reach the water surface. It represents the return from the atmosphere.

L_s, the recorded radiance resulting from the radiation that reaches the water surface, but does not penetrate it. Contains the reflectance from the aquatic surface.

L_v, the portion of the radiation that reaches, and trespasses the water surface and re-emerges from the water column without encountering the bottom of the natural water body. Represents the return from the volume of the water column.

L_b, the portion of the radiation that penetrates the water column reaching the bottom of the water body, and re-emerges from the water column. Represents a return from the bed of the natural water body.

The major target in climatology, meteorology, oceanography, and hydrology projects is the surface layer (L_s), which gives the spectral response of the surface water´s body

characteristics. And so, the most used AOP property is the remote sensing reflectance (R_{rs}), defined as the ratio of water-leaving radiance to downwelling irradiance (E_{sky} and E_{sun}),(D. R. Mishra et al., 2017).

The color of natural waters that gives this spectral response is determined by the concentrations of dissolved and suspended colored compounds. Three main components alter the color in inland or continental waters: (1) colored dissolved organic matter (CDOM), (2) sediment load (total suspended material, TSM), and (3) gross biological activity (estimated generally through the chlorophyll-a concentration, Chl-a). These components are important water quality indicators (IOCCG, 2000).
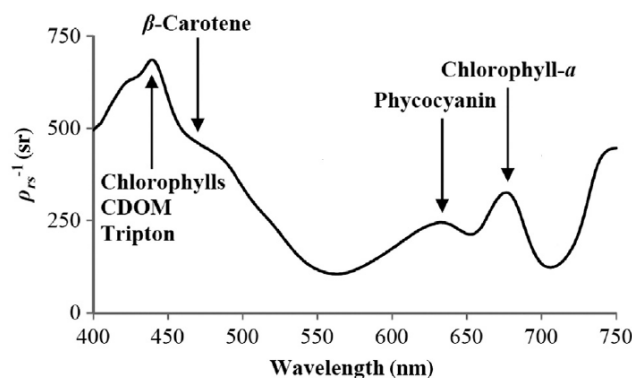
Figure 7. Typical inland waters inverse Rrs spectrum. The positions of the absorption peaks by constituents, such as Chl-a, PC, and CDOM are labeled. Source: Taken from (D. R. Mishra et al., 2017).

Since water is highly absorptive within the near and shortwave infrared spectrum, the majority of water-leaving radiance occurs within the visible spectrum with slight variations dependent on temperature and salinity (Topp et al., 2020b). Figure 6 shows the spectral responses for some of these compounds, in the graphic the absorption peak around 675 nm wavelength is related to the absorption by Chl-a, and there is a high absorption in the blue spectral region due to the combined absorption by phytoplankton pigments, β-Carotene, and CDOM.

1.2.1.1. Chlorophyll -a

Chlorophylls are photosynthetically active compounds that convert light into energy for photosynthesis. Remote sensing studies primarily focus on chlorophyll-a (Chl-a), which is the most abundant chlorophyll and is present within all plants, algae, and cyanobacteria that photosynthesize (Topp et al., 2020b), as it is considered an indicator of phytoplankton

abundance and biomass production in lake waters, it can be used to determine the water quality, biophysical status, and therefore the trophic state level of a water body (Ha et al., 2017).

For low biomass, oligotrophic to mesotrophic water bodies, the Chl-a spectrum is characterized by a sun-induced fluorescence peak around 680 nm. For high biomass, eutrophic water bodies, the fluorescence signal is masked by absorption features and backscatter peaks centered at 665 nm and 710 nm respectively (Topp et al., 2020b).

After the identification of the wavelength range for Chl-a absorption, several models have been developed for the estimation of Chl-a concentration in inland waters (Gurlin et al., 2011; Ha et al., 2017; D. R. Mishra et al., 2017), using a wide range of sensors, resulting in various empirical, semi-empirical and analytical logarithms.

1.2.2. Earth Observation Sensors

For remote sensing projects in aquatic environments, several sensors have been used which focus primarily on passive satellite sensors, the most common open source are shown in Table 2, differentiating whether they work for inland water bodies or oceanic waters. These, vary in their applicability, based largely on their spatial, temporal, spectral, and radiometric resolutions (Topp et al., 2020b).

Table 2. Most used open-source sensors available for monitoring aquatic environments.

Type	Sensor	Satellite	Operation	Space Agency	Spatial Resolution	Monitoring target
Oceanic waters sensor	MODIS (Moderate Resolution Imaging Spectroradiometer)	Terra	1999 -	NASA	1 km	Ocean Color, phytoplankton estimation, biogeochemistry
		Aqua	2002 -			
	MERIS (Medium Resolution Imaging Spectrometer)	Envisat -1	2002 -	ESA	300 m/ 1.2 km	Ocean Biophysical Properties, Coastal Waters, hydrology.
	OLCI (Ocean and Land Cover Instrument)	Sentinel -3	2019 -	ESA	300 m	Ocean and land surface biological properties.
	SeaWIFS (Sea-Viewing Wide Field-of-View Sensor)	OrbView-2	1997 - 2010	NASA	1.1 km	Ocean color dynamics.

Type	Sensor	Satellite	Operation	Space Agency	Spatial Resolution	Monitoring target
	ASAR (Advanced Synthetic Aperture Radar)	Envisat - 1	2002 -	ESA	30 m /1.2 km	Ocean dynamics
Land surface sensor	MSS (Multispectral Scanner)	Landsat 1-5	1972 - 2013	NASA	80 m	High-resolution, multispectral data of the Earth's surface
	TM (Thematic Mapper)	Landsat 4-5	1982 - 2013	NASA	30 m/ 120m	High-resolution, multispectral data of the Earth's surface
	ETM+ (Enhanced Thematic Mapper)	Landsat 7	1999 -	NASA	15m PAN 30m VNIR 60m TIR	High-resolution, multispectral data of the Earth's surface
	OLI (Operational Land Imager)		2013 -	NASA	15 m PAN 30m(VIS/NIR/SWIR)	High-resolution, multispectral data of the Earth's surface
	MSI (Multispectral Instrument)	Sentinel - 2 A/B	2015 -	ESA	10m/ 20m	High-resolution, multispectral data of the Earth's surface

Source: NASA official website for Landsat missions, ESA official website for Sentinel for Copernicus missions.

However, in general, land surface sensors have a finer spatial resolution (~10-30m), that allows them to detect spatial patterns of water quality in small-scale water bodies (e.g., small lakes and rivers), which is the reason to chose Sentinel 2 and Landsat 8 imagery to carry out this project.

The Sentinel-2 satellite belongs to the Copernicus Program (European Commission and European Space Agency), which has on-board the MultiSpectral Instrument (S2A/B-MSI). Though S2A/B-MSI was designed for land studies, it is possible to use it for water studies thanks to its optimized spatial resolution (10-20 m), good radiometric resolution, adequate band configuration, and short revisit time (5 days using the Sentinel-2A and Sentinel-2B satellites at the equator and 2-3 days at mid-latitudes) (Pereira et al., 2020), which makes it an ideal instrument for remote monitoring of lakes and reservoirs with reduced surface area, as Fúquene Lagoon which is approximately 30 km^2.

Landsat 8, as a counterpart, is a satellite launched as a collaboration between NASA and the USGS (United States Geological Survey), that provides multispectral satellite images from the Earth through its sensor, Operational Land Imager (OLI), with a special resolution of 30m, and a revisiting time of 16 days (USGS, n.d.). The red, near-infrared (NIR), and shortwave

infrared (SWIR) bands in this satellite have a narrower bandwidth than in previous Landsat missions, as well as a better radiation resolution, improving its pigment discrimination ability(Buma & Lee, 2020). Similar case than with Sentinel-2, even though Landsat 8 was built for terrestrial applications, its bands have proven useful for estimating concentrations of Chl – a in water bodies (Page et al., 2019; Pahlevan et al., 2014; Watanabe et al., 2018).

2. METHODOLOGY
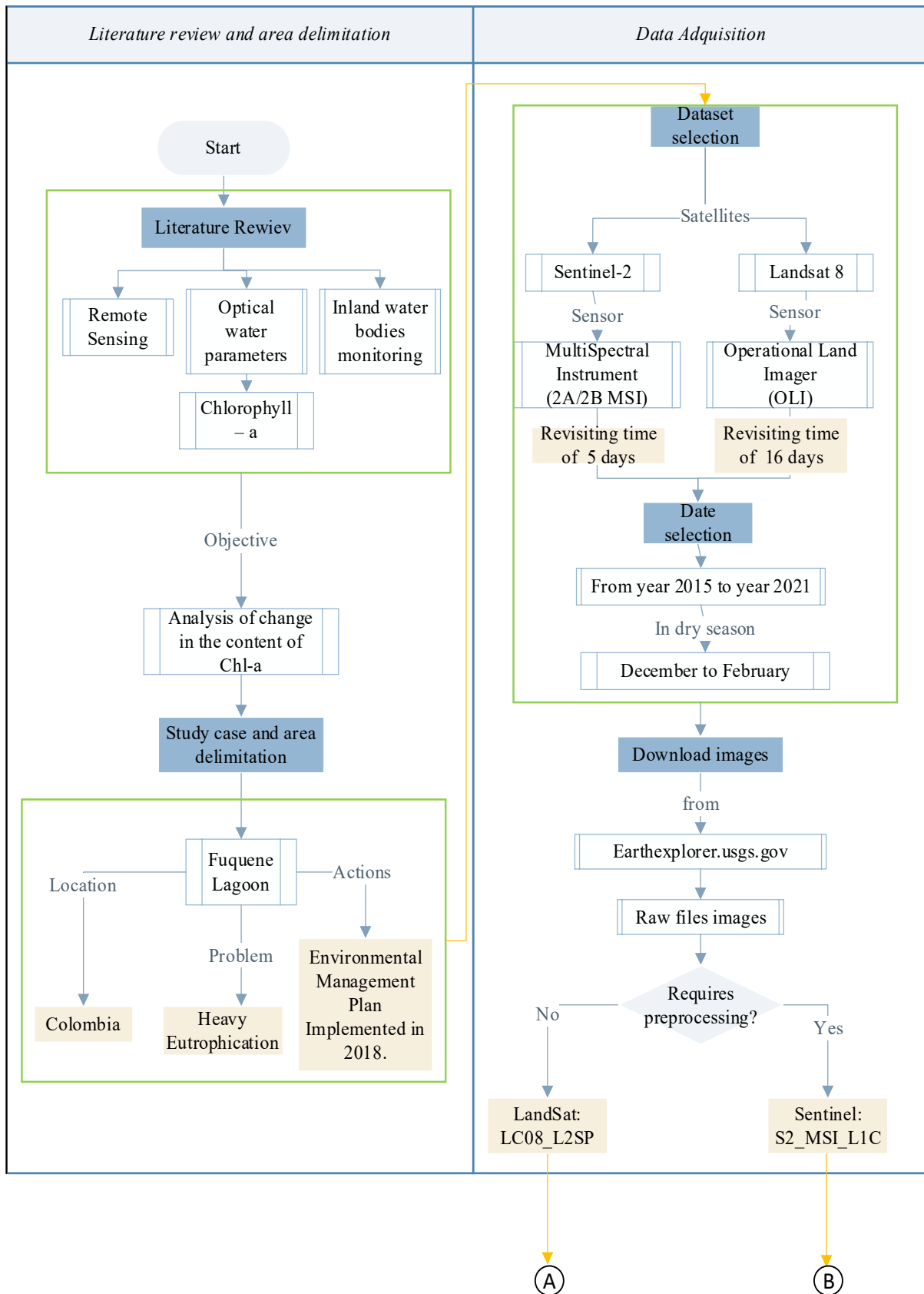
Figure 8. Flowchart of the methodology followed 1/2. Source: Created by the author.
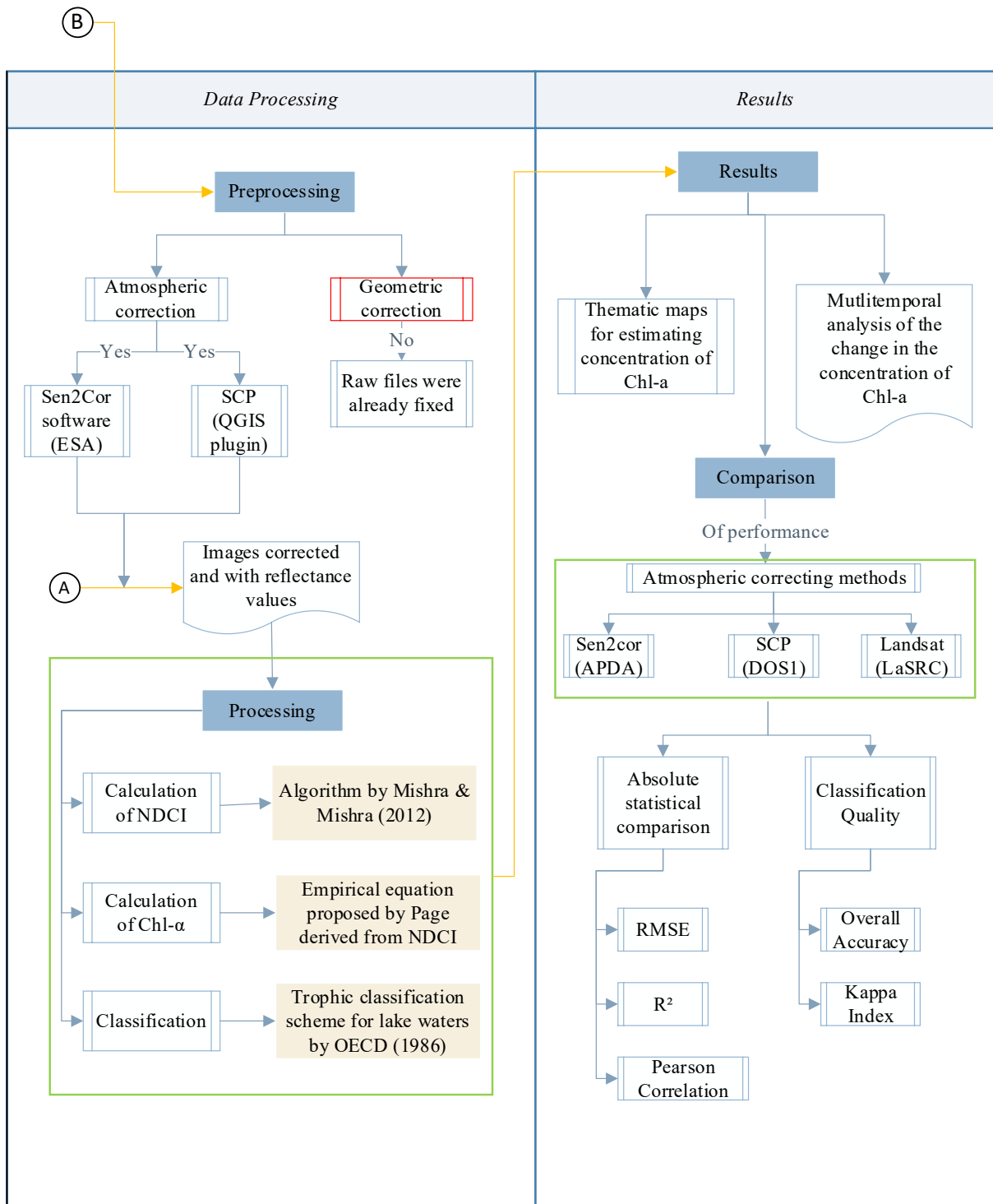
Figure 9. Flowchart of the methodology followed 2/2. Source: Created by the author.

The methodology was divided into four stages, presented in (Figure 8 and Figure 9). The first stage was the literature review of the use of remote sensing technologies in the identification of water quality parameters for freshwater bodies. After that, the study case was selected in order to proceed with the satellite imagery acquisition. The imagery was processed

in the geographic information software QGIS (v3.16 Hannover); finally, the results were collected and analyzed.

The following is a detailed description of the methodology used in the project.

2.1. Study Case

Fúquene Lagoon was chosen as the case study for this investigation as the water body is now under an environmental management plan to recover its surface as well as regulate its chemical and physical properties, and so a fast way to estimate Chlorophyll-a content would contribute to this objective. The lagoon is a freshwater body of tectonic origin located to the east of Colombian Andes, in the municipality of Fúquene, between the departments of Cundinamarca and Boyacá (Figure 10). It is placed at 2543 m.a.s.l of altitude. Its geographic location is amongst latitude 5º 29'50''N; 5º 25'26''N, and longitude 73º 46'49''O; 73º 42'44'' O (Castillo & Rodríguez, 2017).
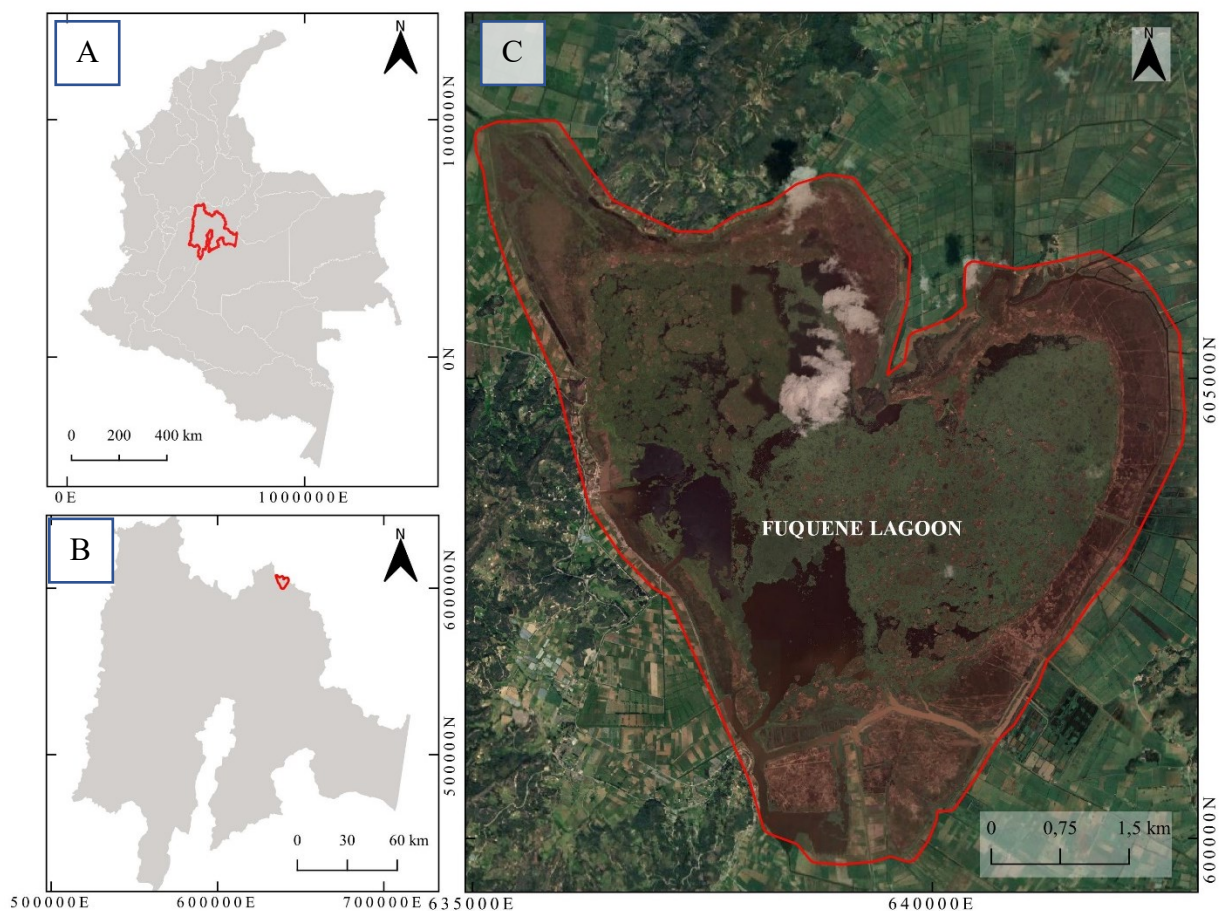

*Figure 10. Fúquene Lagoon location. A) Location of Cundinamarca department in Colombia. B): location of Fúquene Lagoon in Cundinamarca context.*Geographic Projection: WGS84 / UTM zone 18N. Source: Created by the author*

The area is characterized by two dry seasons and two wet seasons, that alternate between each other. Dry seasons occur from months December to February and from months June to August, while wet seasons happen during months March to May and September to November. The yearly average rainfall is 850 mm, and the average temperature is between 12 and 13.2°C (Castillo & Rodríguez, 2017).

The lagoon was one of the most important hydric ecosystems of the region with a water surface of nearly 100 km^2 (CAR, 2018); however, over the last decades, that surface has been decreasing to only 32 km^2, and due to the 6,700 tons of sediment that enter the lagoon every year, the water level has also been reduced more than one meter.

The previously has happened as a result of several factors like the continuous depletion of water inflow of the tributaries, the water withdrawal for irrigation of the growing agricultural areas, as well as untreated wastewater and nutrient intake from animal husbandry that has caused strong eutrophication of the water leading to the massive growth of aquatic vegetation like water hyacinth (*Eichhornia crassipes*) and Egeria (*Egeria densa*) (Global Nature Fund, 2011).

Currently, the lagoon belongs to the Cundinamarca Regional Autonomous Corporation (CAR by its initials in Spanish) jurisdiction, which is the environmental regional authority for the management of natural resources and sustainable development in Colombia. Additionally, the lagoon is part of an especial area of management denominated Regional District of Integrated Management for Fúquene, Cucunubá, and Palacios lagoons (DRMI by its Spanish initials). The lagoons network supplies water for domestic, agricultural, livestock, and industrial demand for over 650.000 inhabitants; besides being the habitat for several migratory and endemic species, as well as offer various environmental services to the local population (CAR, 2018).

Figure 11. Cleaning processes carried out in Fúquene Lagoon in the year 2020. Source: Taken from CAR website.

Due to its importance, in the year 2018, an environmental assessment plan was proposed for the DRMI Fúquene, Cucunubá, and Palacios, which was implemented in the mid-year 2019 to improve and recovery the hydric equilibrium of the ecosystem, Figure 11 shows some of the cleaning activities in the lagoon. The plan includes a complete program of monitoring the air, soil, and water variables. For the latter, water quality monitoring is done employing eight sensors with multi-parameter probes that measure: temperature, conductivity, pH/ORP (oxidation-reduction potential), turbidity, dissolved oxygen; as well as nitrogen ions, chlorine, and chlorophyll content.

2.2. Acquisition of Satellite Data and Preprocessing

For this research, images from Sentinel-2, and Landsat 8 satellites were used due to the open access facility, high resolution, and temporal availability. The datasets were downloaded from the website Earth Explorer (https://earthexplorer.usgs.gov/), which is the official data portal for geospatial products of the United States Geological Survey (USGS).

The specifications of Sentinel-2 bands and Landsat 8/OLI bands used in this study are presented in Table 3 (ESA, 2020a; USGS, 2018).

Table 3. Datasets and band specifications used for this research.

Satellite	Band	Central wavelength (nm)	Wavelength (nm)	Resolution (m)
Sentinel -2	B02 - Blue	492.4	458 - 523	10
	B03 - Green	559.8	543 - 578	10
	B04 - Red	664.6	650 - 680	10
	B05 - Red Edge 1	704.1	698 - 713	20
Landsat 8 - OLI	B02 - Blue	482.6	450 - 510	30
	B03 - Green	561.3	530 - 590	30
	B04 - Red	654.6	640 - 670	30
	B05 - NIR	864.6	850 - 888	30

Images available from the year 2015 until the year 2021, were downloaded for both satellites for the dry season of the study area (December to February) in order to avoid any

significant hydrological event like rain that could change the chemistry of the water and its quality in the season analyzed (Yigit Avdan et al., 2019); except for the year 2017, where the cloud coverage did not provide any acceptable visibility of the lagoon. In total 28 images (eighteen from Sentinel-2 and ten from Landsat 8), displayed in Table 4, were suitable and used in the consequent analysis.

Table 4. Satellite imagery used.

Satellite/ Sensor	Acquisition Date (Year_Month_Day)	Grid ID	Satellite/ Sensor	Acquisition Date (Year_Month_Day)	Grid ID
Sentinel-2A MSI	2015_12_21*		Landsat 8 OLI	2015_01_04	
Sentinel-2A MSI	2016_01_10*		Landsat 8 OLI	2015_12_22*	
Sentinel-2B MSI	2018_01_24		Landsat 8 OLI	2016_01_07*	
Sentinel-2A MSI	2018_12_15		Landsat 8 OLI	2016_01_23	
Sentinel-2A MSI	2018_12_25		Landsat 8 OLI	2016_11_22	Path: 008 Row: 056
Sentinel-2B MSI	2018_12_30*		Landsat 8 OLI	2018_12_30*	
Sentinel-2A MSI	2019_01_04		Landsat 8 OLI	2019_02_16*	
Sentinel-2A MSI	2019_02_03	T18N XM	Landsat 8 OLI	2019_12_17	
Sentinel-2A MSI	2019_02_13*		Landsat 8 OLI	2020_01_02*	
Sentinel-2A MSI	2019_12_10		Landsat 8 OLI	2021_03_09*	
Sentinel-2B MSI	2020_01_04*				
Sentinel-2A MSI	2020_01_09				
Sentinel-2B MSI	2020_01_14				
Sentinel-2B MSI	2020_02_13				
Sentinel-2A MSI	2020_02_18				
Sentinel-2A MSI	2020_12_04				

Satellite/ Sensor	Acquisition Date (Year_Month_Day)	Grid ID	Satellite/ Sensor	Acquisition Date (Year_Month_Day)	Grid ID
Sentinel-2A MSI	2021_01_13				
Sentinel-2B MSI	2021_01_18*				

* Datasets used for comparing purposes of both Sentinel-2 and Landsat 8 satellites.

The raw files for Sentinel-2 images were downloaded as MSI – Level 1C, which is a file with a level of preprocessing that provides Top-Of-Atmosphere (TOA) reflectance values with a corrected geometry that needs to be processed again to obtain Bottom-Of-Atmosphere (BOA) reflectances to remove any intervening atmospheric effects from the acquired Sentinel images. For this stage, the software Sen2cor was used, which is provided by the European Space Agency (ESA). This one performs the atmospheric-, terrain and cirrus correction of TOA Level 1C input data, to achieve BOA Level 2C product (ESA, 2020b), using the algorithm named Atmospheric Precorrected Differential Absorption (APDA), for the spatial resolutions of 10, 20, and 60 m respectively (Louis et al., 2016).

For Landsat 8 OLI images, Collection 2 Level 2 Science Products (L2SP) files were downloaded. These have been already corrected by a software called Land Surface Reflectance Code (LaSRC), delivering surface reflectance data products (Jenkerson, 2020), so there was no need for extra preprocessing steps.

In addition to the previously named preprocessing steps, for comparison purposes, the Dark Object Subtraction (DOS) method for atmospheric correction was also tested for Sentinel -2 imagery, using the QGIS® plugin SCP (Semiautomatic Classification Plugin). DOS is an image-based technique in which the basic assumption is that within the image some pixels are in complete shadow and their radiances received at the satellite are due to atmospheric scattering (path radiance). This assumption is combined with the fact that very few targets on the Earth's surface are absolute black, so an assumed one-percent minimum reflectance is better than zero percent (Chavez, 1996). It is worth pointing out that the accuracy of image-based techniques is generally lower than physically-based corrections.

Despite having different revisiting schedules, with the aim to compute and display the comparison and correlation existing between the results given by both satellites, a pair of

datasets were chosen per year considering a similar date range for Sentinel 2 and Landsat 8. In Table 4, the datasets selected can be identified by the (*) symbol in the field of acquisition time.

2.3. Processing

In this stage, the raster files of the bands obtained from the previous step were used to calculate Normal Difference Chlorophyll Index (NDCI) and Chlorophyll content (Chl – α). All of the calculations were processed in the geographic information system software QGIS® 3.16.4 (Hannover), using the graphic model builder tool to create a model per each algorithm in order to facilitate the process and automatized iterations per each dataset.

2.3.1. NDCI

NDCI was calculated using the equation *(2)*, proposed by (S. Mishra & Mishra, 2012) to estimate Chl – α content in turbid waters (case 2) as a standardized algal index,

$$NDCI = \frac{[R_{rs}(708) - R_{rs}(665)]}{[R_{rs}(708) + R_{rs}(665)]} \qquad (2)$$

Where R_{rs} is the remote sensing reflectance, in this case, the surface reflectance obtained from the atmospheric correction methods in preprocessing. NDCI can be rewritten in the function of the bands 4 and 5, as shown in equation *(3)*, for both Sentinel -2 and Landsat 8 satellite band imagery, as stated by (Buma & Lee, 2020).

$$NDCI = \frac{[Band\ 5 - Band\ 4]}{[Band\ 5 + Band\ 4]} \qquad (3)$$

Figure 12 displays the graphic model built in QGIS® 3.16.4 (Hannover), where the input data were bands 4 and 5, and the raster calculator tool was used to operate equation *(3)*. The next step was to clip the resulting NDCI raster to the area of Fúquene Lagoon.
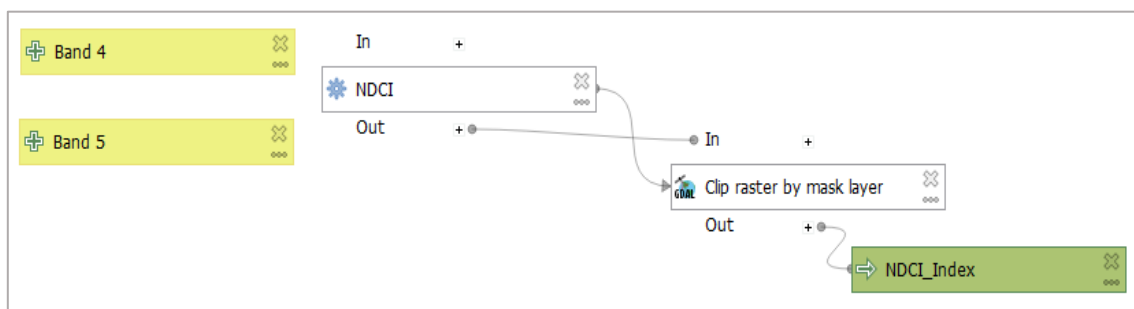

Figure 12. NDCI algorithm graphic model. Source: Created by the author.

2.3.1. Chlorophyll – a

An empirical algorithm *(4)* derived from NDCI to retrieve Chl – α concentration was used in this step. The algorithm was first proposed by (Page et al., 2018) in their study for the Utah Lake in the U.S., and later validated by (Pereira et al., 2020) for tropical regions as Brazil, where the resulting concentration of chlorophyll is given in $\left(\frac{mg}{m^3}\right)$ or $\left(\frac{\mu g}{L}\right)$.

$$Chl - \alpha = 14.039 + 86.115\,(NDCI) + 194.325\,(NDCI)^2 \qquad\qquad (\,4)$$

Figure 13 shows the graphic model made for this algorithm. Here, for Sentinel -2 images there was an extra step to resample the spatial resolution from 20m to 30m, to be able to perform a comparison with the Landsat 8 imagery since they only come in 30 m spatial resolution. The downscaling was chosen since it has been shown to have superior performance compared to upscaling in Sentinel -2 imagery, even when based on the most straightforward technique, the nearest neighbor resampling (Lima et al., 2019).
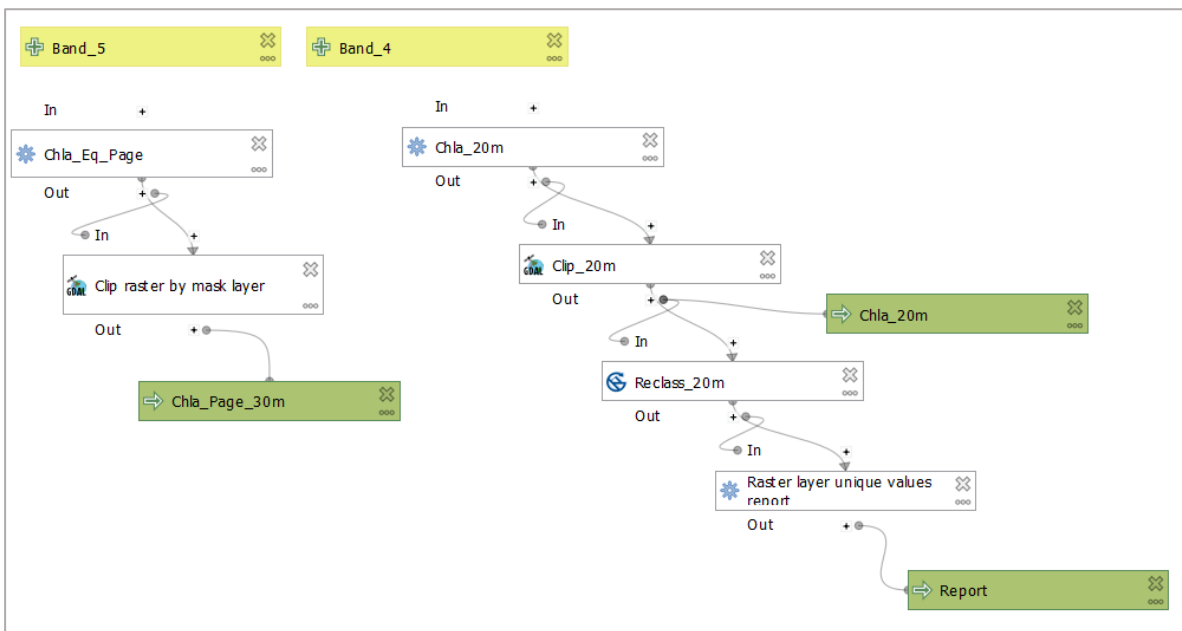

Figure 13. Graphic model for Chl-a. Source: Created by the author.

2.3.2. Classification

The resulting rasters were reclassified following a threshold classification scheme proposed by the Organisation for Economic Co-operation and Development (OECD) for the assessment and control of eutrophication in inland water bodies.

This scheme (Table 5) defines the five traditional trophic categories by setting boundaries for the annual average values for total phosphorus, chlorophyll, and water transparency, and for the maximum and minimum values for the latter two parameters. These are the three key parameters in assessing the level of eutrophication and its effects. Inputs of phosphorus to freshwaters commonly result in planktonic algal and cyanobacterial growth, which are most easily quantified by measurement of the algal pigment chlorophyll. Water transparency is an important aesthetic characteristic in lakes and frequently determines the suitability of a waterbody for recreational pursuits such as game fishing and swimming. It is reduced by the presence of suspended material, such as planktonic organisms, in the water column (OECD, 1982).

Table 5. Trophic Classification scheme for lake waters proposed by O.E.C.D.

Lake Category	Total Phos. (mg/m3)	Chlorophyll (mg/m3)		Transparency m	
	Mean.	Mean.	Max.	Mean.	Max.
Ultra - Oligotrophic	<4	<1.0	<2.5	>12	>6
Oligotrophic	<10	<2.5	<8.0	>6	>3
Mesotrophic	10 – 35	2.5 – 8	8 – 25	6 – 3	3 – 1.5
Eutrophic	35 – 100	8 – 25	25 – 75	3 – 1.5	1.5 – 0.7
Hypertrophic	>100	>25	>75	<1.5	<0.7

For this particular study, only the Chlorophyll parameter is estimated, and as Fúquene Lagoon is, an already hyper-polluted water body, the classification threshold carried out does not contemplate an ultra-oligotrophic state, working with only 4 categories from Table 5, oligotrophic, mesotrophic, eutrophic, and hypertrophic states.

2.3.3. *Comparison and correlation of results*

As mention before, atmospheric correction plays an important role when estimating optical properties from the water in remote sensing techniques, here the main two atmospherical correction methods for Sentinel-2 and Landsat 8 were compared, APDA and LaSCR respectively. In addition to the DOS method for Sentinel-2 imagery.

There were two instances for comparison and correlation, the first one made between Sentinel-2 results versus Landsat 8 results, using the default atmospherical correction methods recommended by the ESA and the USGS, which were APDA (algorithm obtained through the software Sen2cor), and LaSCR respectively.

In the second instance, Sentinel-2 results were compared given the performance of the previously mention atmospheric correcting method, and the less refined DOS method, following the same methodology of processing for the estimation of Chl-a.

For these two cases, an absolute statistical comparison pixel-to-pixel was made with an image regression process, computing the Pearson correlation coefficient, R^2 determination coefficient, and root mean square error (RMSE), for these coefficients the WhiteBox Tools® software was used, as a standalone version. In addition, to measure the accuracy of the classification threshold, a confusion matrix was computed taking 250 random points from the baseline or ground truth to get the Kappa Index, which is a measure of reliability for qualitative (categorical) items; and the overall accuracy index. For the latter two, the Orfeo Toolbox® software was used, as a standalone version as well.

In all of the previous cases, Sentinel-2 images corrected with the APDA method were chosen as a baseline or independent variable, since it was not possible to obtain in situ measurements from Chl-a in Fúquene Lagoon. And, assuming that these images had better and more accurate results since they have the band 5 with reflectance peak centered at 705 nm, which is the maximally sensitive peak to the variations in Chl-a concentration in water (S. Mishra & Mishra, 2012).

3. RESULTS AND DISCUSSIONS

3.1. Sentinel -2

Figure 15, Figure 17, Figure 16, and Figure 17 present the thematic maps resulting from the calculated Chl-a concentration using the empirical algorithm in equation *(4)* for Sentinel-2 images, these were atmospherically corrected with Sen2cor software with APDA algorithm. Each map corresponds to the date of acquisition displays in Table 4 and is presented with geographic projection WGS84 / UTM zone 18N.
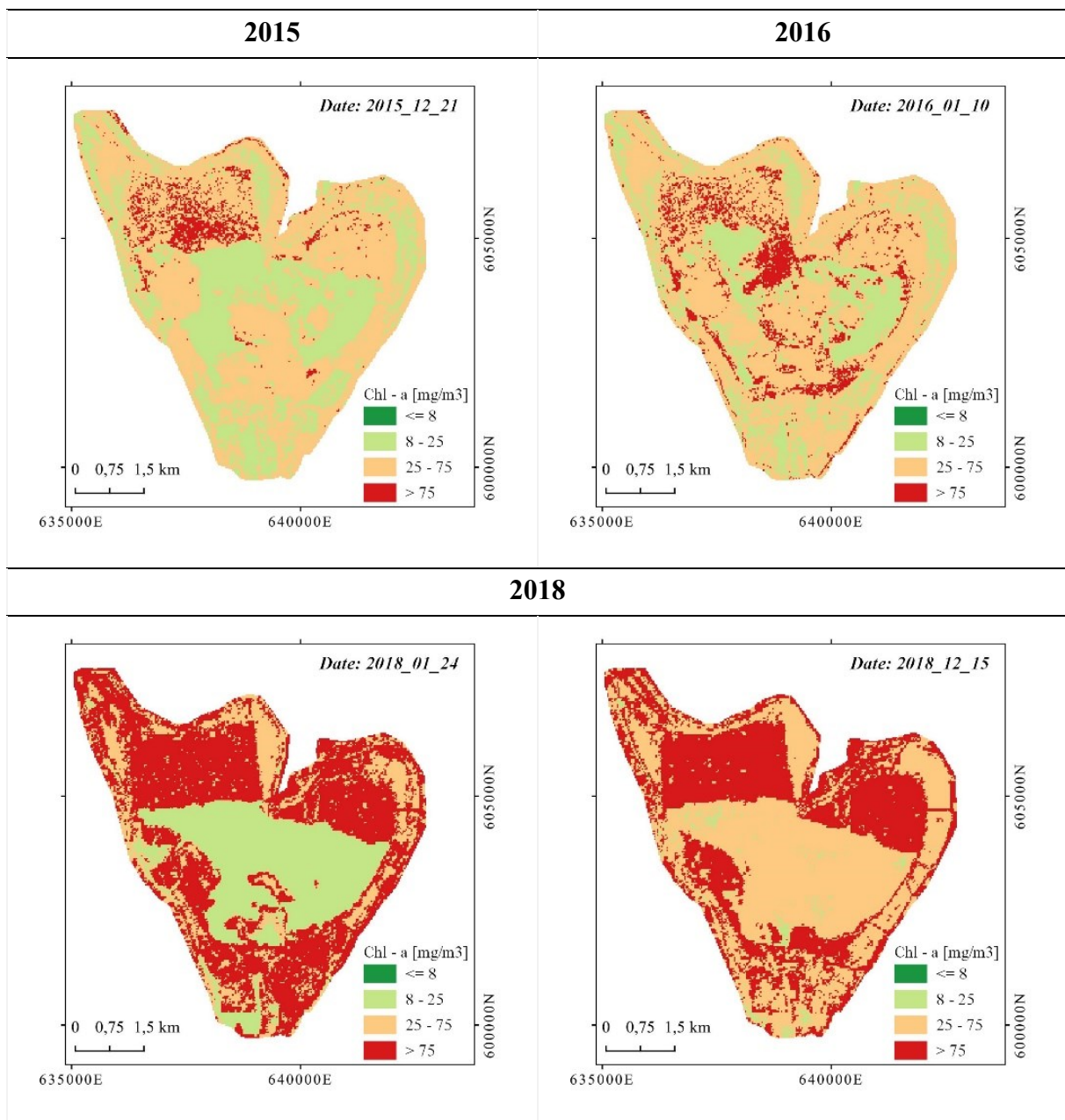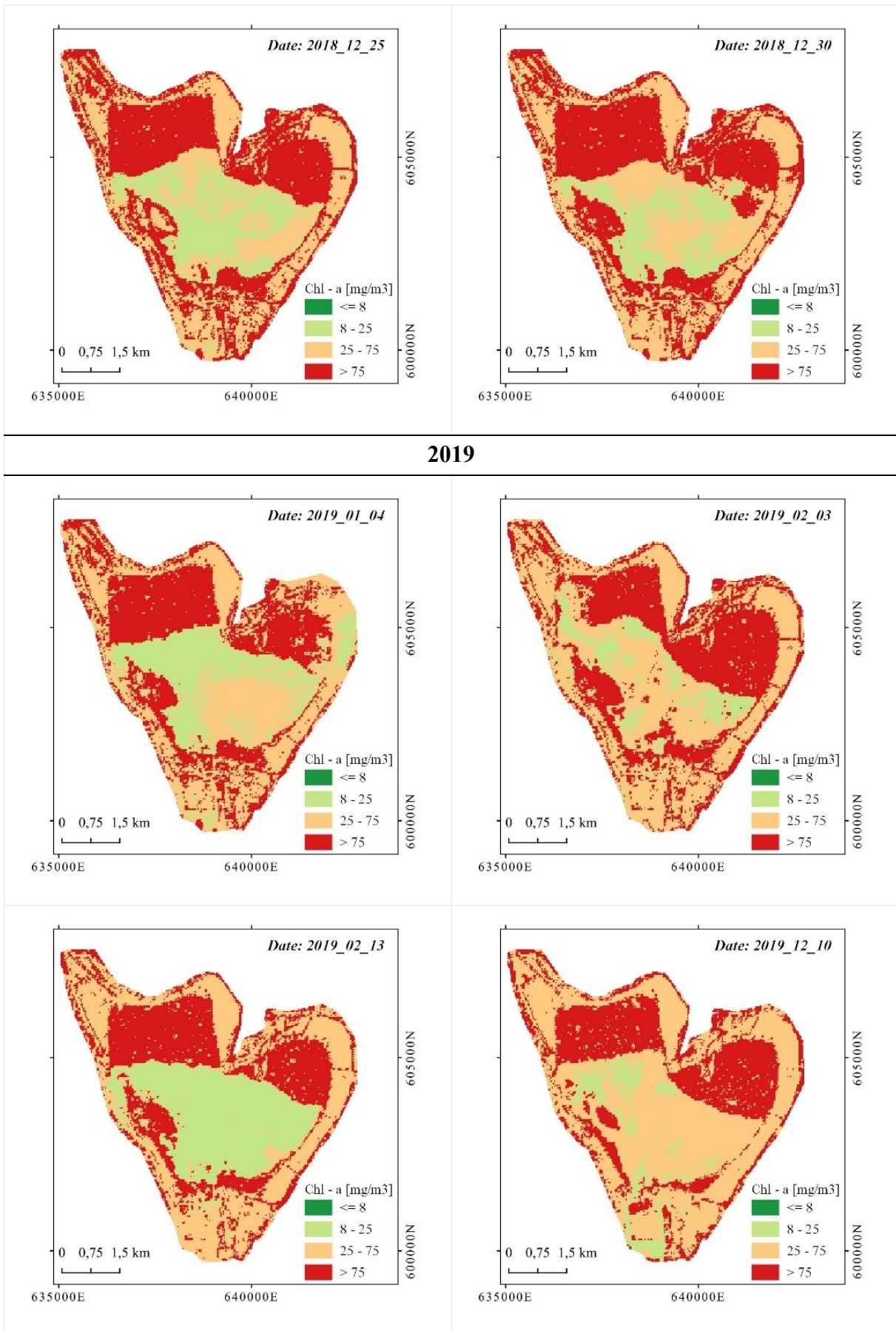

Figure 14. *. Thematic maps for Chl-a estimation in Sentinel-2 imagery (1/4).*

Figure 15. *Thematic maps for Chl-a estimation in Sentinel-2 imagery (2/4).*
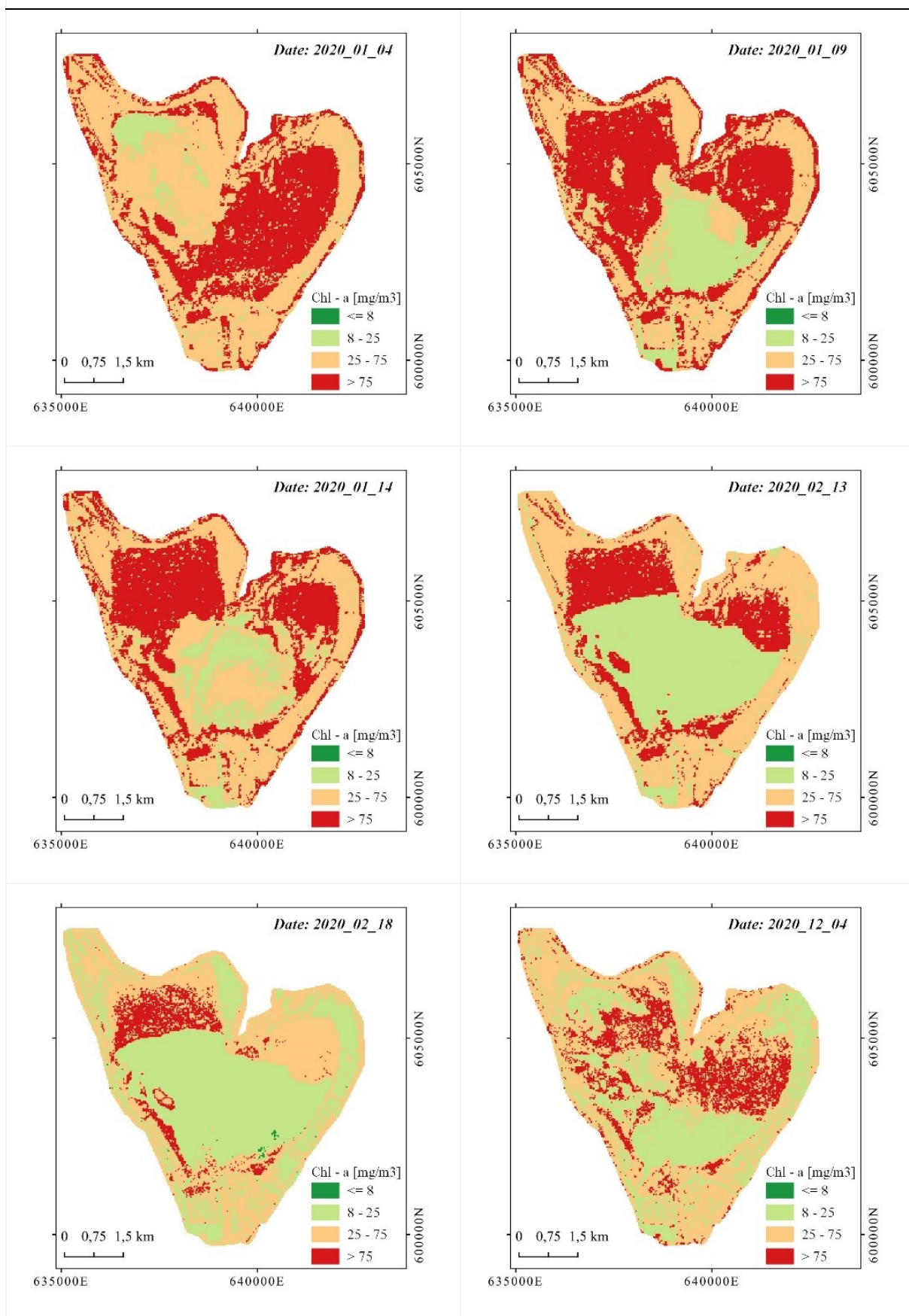
2020

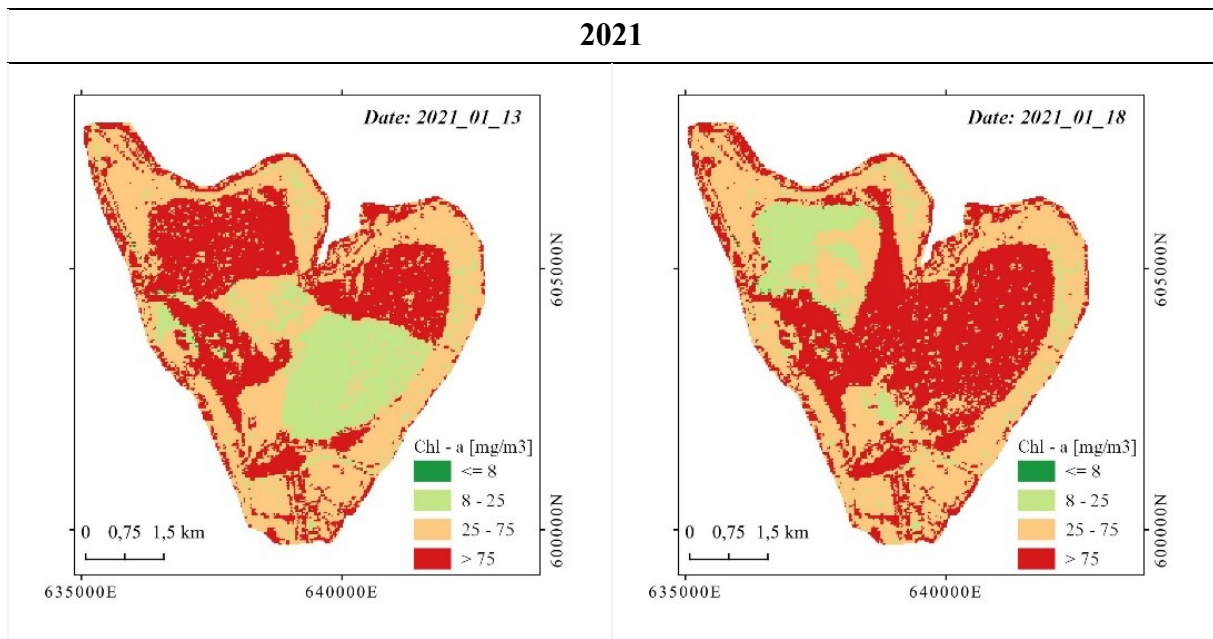*Figure 16. Thematic maps for Chl-a estimation in Sentinel-2 imagery (3/4).*

Figure 17. Thematic maps for Chl-a estimation in Sentinel-2 imagery (4/4).

3.2. Landsat 8

Figure 18, Figure 19, and Figure 20 display the thematic maps resulting from the Landsat 8 images for the Chl-a concentration. The atmospheric correction method used was the default given by the USGS, LaSRC, and same as with Sentinel-2 results, the maps are presented with geographic projection WGS84 / UTM zone 18N.
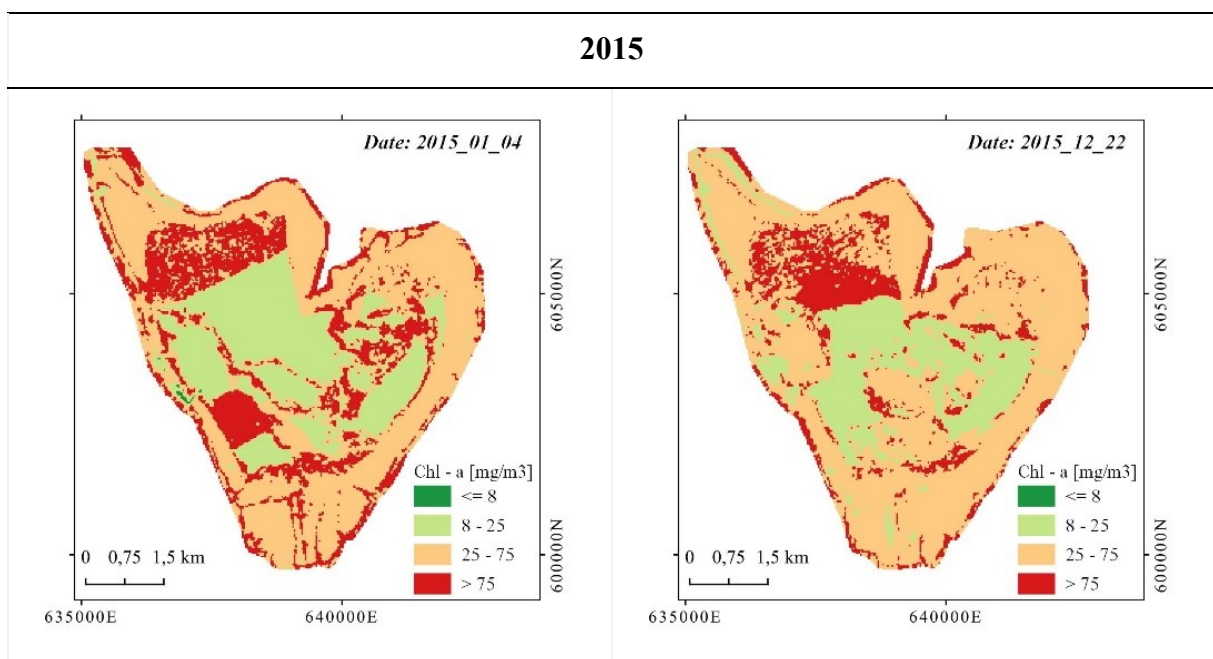
2015

Figure 18. Thematic maps for Chl-a estimation in Landsat 8 imagery with LaSCR (1/3)
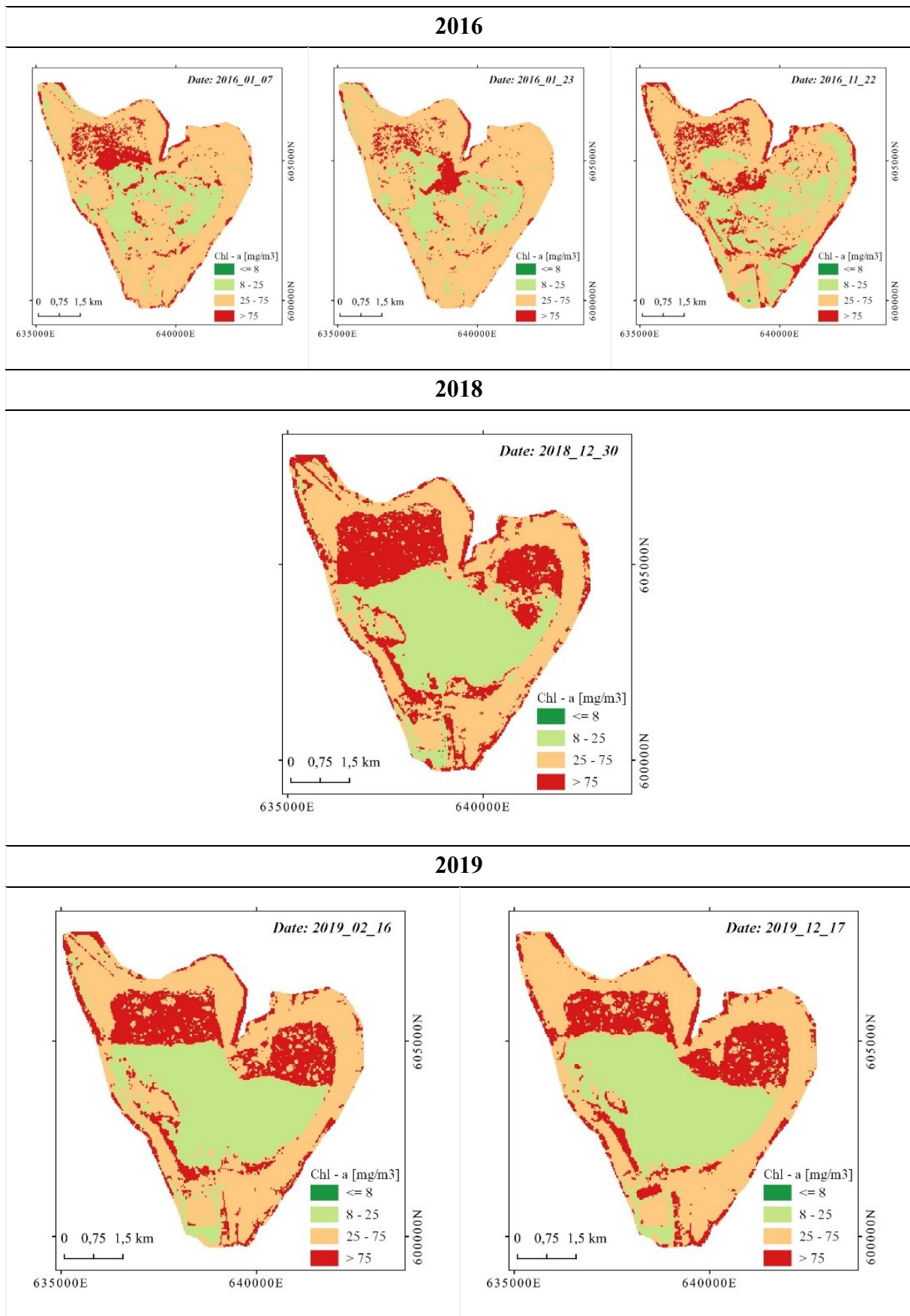
2016

2018

2019

Figure 19. Thematic maps for Chl-a estimation in Landsat 8 imagery with LaSCR (2/3)
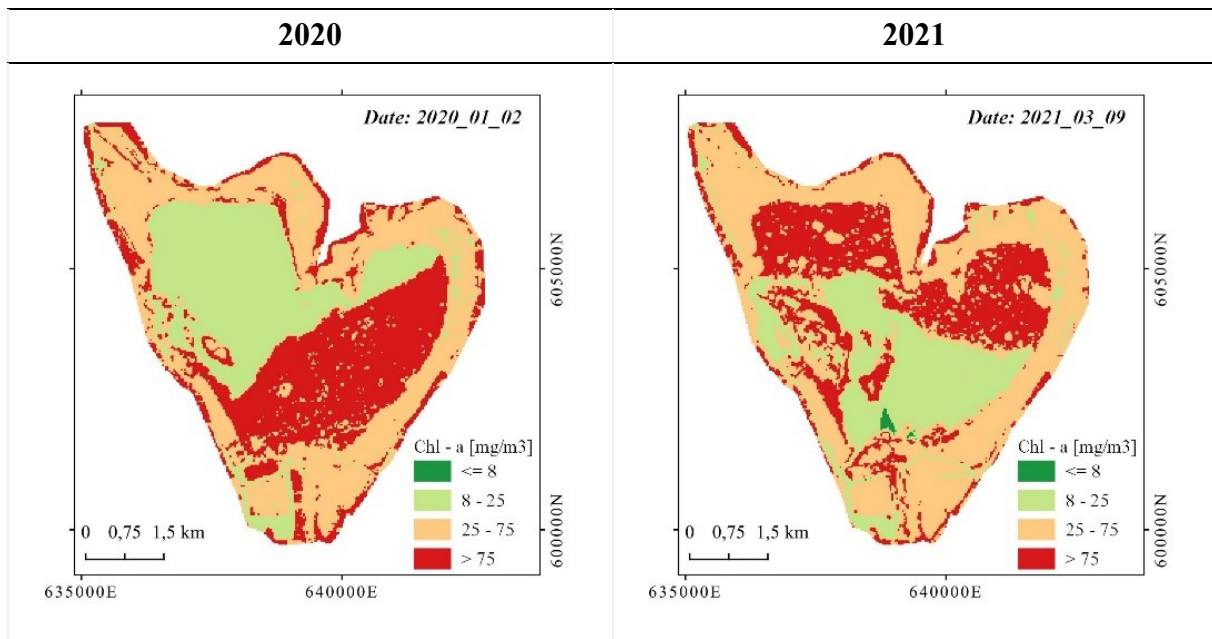
	2020	2021

Figure 20. Thematic maps for Chl-a estimation in Landsat 8 imagery with LaSCR (3/3).

Throughout the previous maps, it is possible to see the dynamic change in the concentration for Chl-a in Fúquene Lagoon, during the years 2015 – 2021, given by the algorithm proposed by Page, see equation *(4)*.

Even though the results do not show any clear pattern regarding the concentration of Chl-a using the classification of trophic states made with OECD guidelines. They do show an increase of biomass content, and therefore eutrophication state of the lake, starting from the year 2018, which can be seen from the results in both satellites, where the red area, identified in the category of the hypertrophic state is considerably bigger than in the immediate available previous results in the year 2016.

To facilitate the visualization of the data, a multitemporal analysis of the change in the areas corresponding to the trophic states of the Fúquene lagoon was made, the compiled statistics results can be seen in Annex 1. Figure 21 and Figure 22 display the area accumulated of each category, for the results from Sentinel-2 and Landsat 8 respectively, during the date frame analyzed.

In Figure 21, it is easier to see how the trophic health of the lake started to decrease even more in 2018, with the growth of areas with the hypertrophic category, identified with the bright red color. This, however, seems to have improved around the year 2020, where the levels of oligotrophic areas grow significantly, represented with the light green color. This could be attributed to the implementation of the environmental assessment plan that started in late 2019.
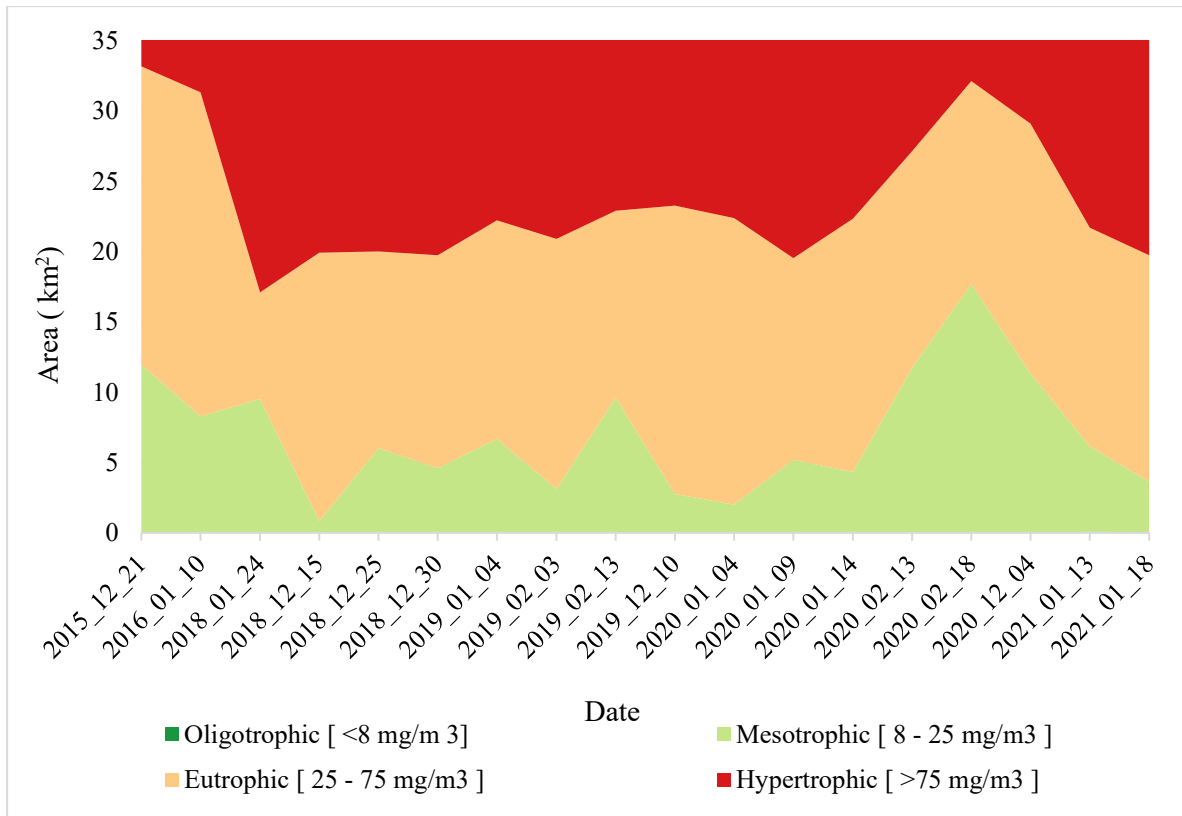
Figure 21. *Temporal change in the accumulated area for the trophic states resulting from Sentinel-2 imagery corrected with APDA method.*
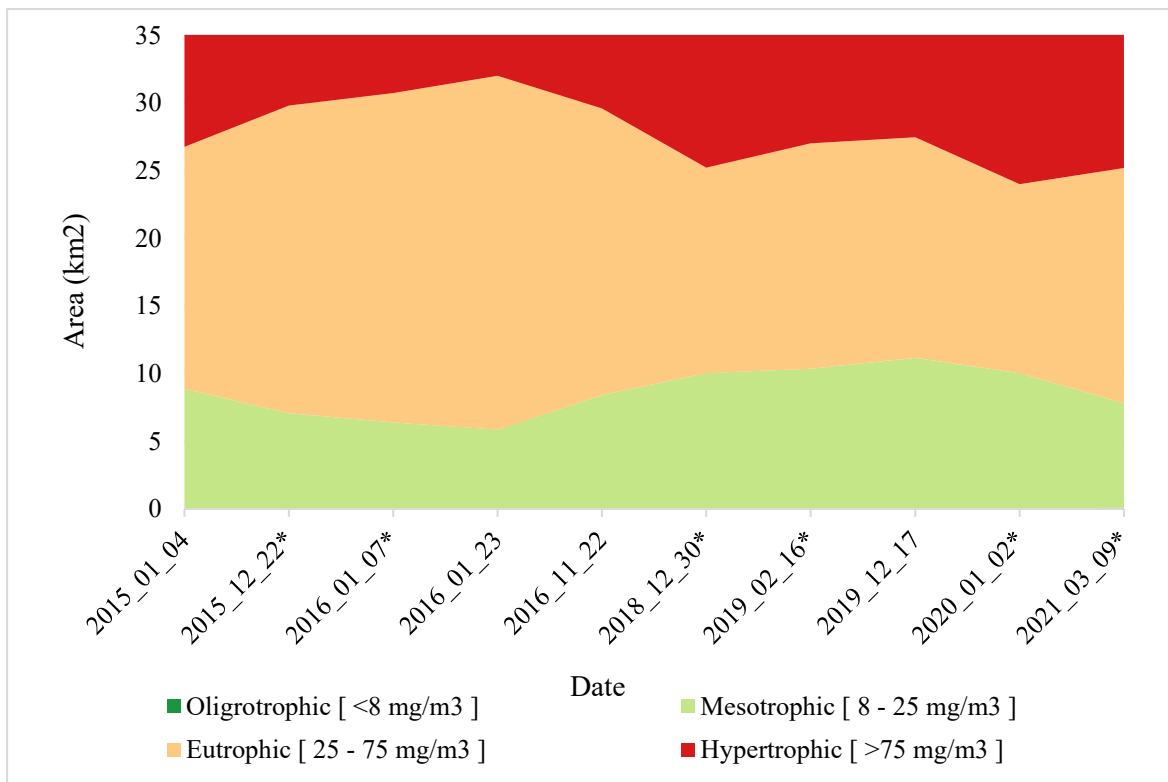

Figure 22. *Temporal change in the accumulated area for the trophic states resulting from Landsat 8 imagery corrected with LaSRC.*

For the Landsat 8 results, in Figure 22, the pattern is somehow similar to the Sentinel-2 one, since is it clear the growth in red areas around the year 2018, and increase of the light green areas around the year 2019 and 2020. However, for this latter date frame, the areas corresponding to hypertrophic state also grow, showing a discrepancy against the Sentinel-2 and Landsat 8 results. But as stated previously, the wavelength used in Landsat 8 is not the closest to the Chl-a peak reflectance, which may have affected the results.

Regarding the previous statement, in Annex 2 a trial was made using band 8A (864.7 nm) in Sentinel-2 imagery in replacement of band 5 (705 nm), to see if maybe a closer band to the Landsat 8 band 5 (864.6 nm), make any significant difference concerning the correlation and comparison of the thematic results, but it did not improve the performance.

3.3. Comparison and correlation

Comparison results were diverse, given the uncertainty existing between the resulting BOA reflectance values obtained by the performance of the atmospherical correction methods compared, APDA, LaSCR, and DOS.
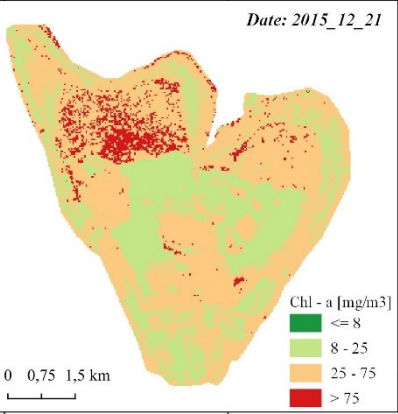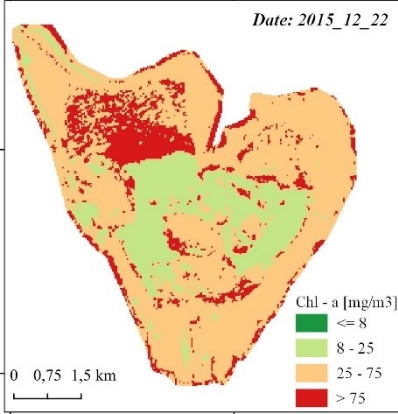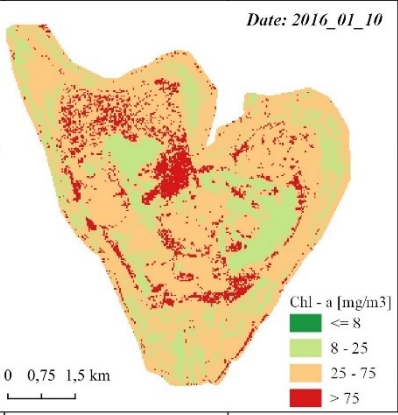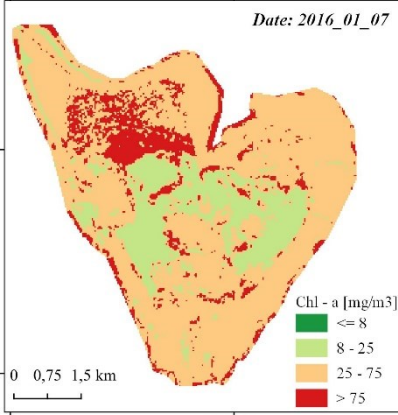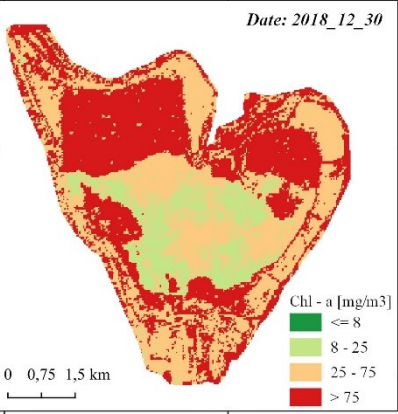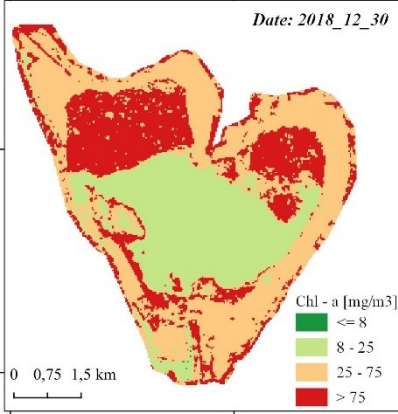
These discrepancies have been addressed in the Atmospheric Correction Inter-Comparison Exercise (ACIX) protocol for Sentinel-2 and Landsat 8 products, where Doxani et al. (2018) give an approach on the complexity of the subject considering the number of atmospheric correction methods created for different purposes. Nevertheless, it is also mention, that LaSCR seems to be one of the best working atmospheric correction methods for Landsat 8 imagery, while Sen2cor seems to give the most accurate results to Sentinel-2 imagery, compared with the real values (Doxani et al., 2018).

3.3.1. Sentinel – 2 (APDA) vs. Landsat 8 (LaSCR).

Table 6 shows the coefficients obtained for the statistical pixel-to-pixel base comparison, the classification accuracy, using Sentinel-2 results corrected with APDA method as "reference" thematic map; and the thematic maps resulting from the estimation of Chl- a for both satellites using the default atmospheric correction methods, in the images chosen to be compared.

In Annex 3 the scatter plot for each pair of datasets can be found, this plot displays in a graphic interface the correlation between the results obtained from both satellites for each pair analyzed.

Table 6. Comparison coefficients between Sentinel-2 and Landsat 8 results for Chl-a estimation.

Sentinel - 2 Corrected with Sen2cor (APDA)	Landsat 8/OLI Corrected with LaSCR	Coefficients
Date: 2015_12_21	Date: 2015_12_22	RMSE= 16.06 R^2= 0.71 Pearson Correlation= 0.84 Kappa=0.50 O.A.=0.74
Date: 2016_01_10	Date: 2016_01_07	RMSE= 19.64 R^2= 0.37 Pearson Correlation= 0.61 Kappa=0.36 O.A.=0.69
Date: 2018_12_30	Date: 2018_12_30	RMSE= 43.36 R^2= 0.53 Pearson Correlation= 0.73 Kappa=0.42 O.A.=0.62
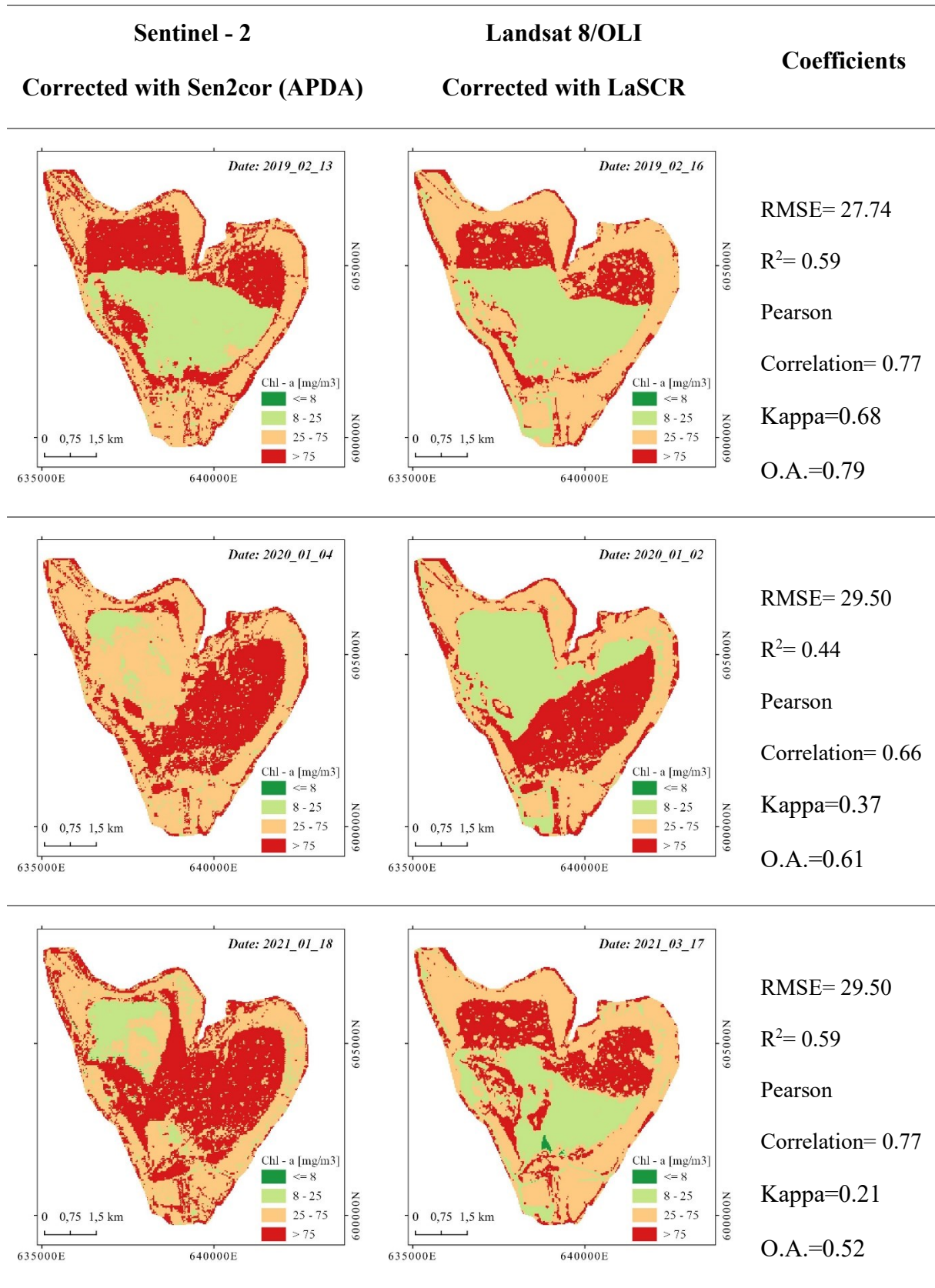
Sentinel - 2 Corrected with Sen2cor (APDA)	Landsat 8/OLI Corrected with LaSCR	Coefficients
 Date: 2019_02_13	 Date: 2019_02_16	RMSE= 27.74 R^2= 0.59 Pearson Correlation= 0.77 Kappa=0.68 O.A.=0.79
 Date: 2020_01_04	 Date: 2020_01_02	RMSE= 29.50 R^2= 0.44 Pearson Correlation= 0.66 Kappa=0.37 O.A.=0.61
 Date: 2021_01_18	 Date: 2021_03_17	RMSE= 29.50 R^2= 0.59 Pearson Correlation= 0.77 Kappa=0.21 O.A.=0.52

O.A.= Overall Accuracy Index, Kappa= Kappa Index, RMSE= Root Mean Square Error, R^2 = Determination r- square coefficient.

Figure 23 displays the resulting coefficients from the comparison between Sentinel-2 and Landsat 8 imagery. When comparing the results, data retrieve from dates of the year 2021 were discarded as they present atypical behavior since the date between one satellite image and the other are not close enough. Having the latter in consideration, with an average determination coefficient R^2 value of 0.53, an average RMSE value of 27.26, and an average Pearson correlation matrix value of 0.72, the results do not exhibit a high level of correlation as expected, and so it might be said there is not an adequate portability of the methodology used in Sentinel-2 images to Landsat 8 images, using the algorithm proposed by Page in the estimation for Chl-a on inland waters. Similar to the previous coefficients, the average Kappa index value was 0.47 and the average overall accuracy value was 0.69, which indicates the classification threshold did not perform as comparable in both satellite imagery, this can also be seen in Table 6 where the thematic maps in Landsat 8 show an underestimation of the Chl-a concentration against the Sentinal-2 ones.
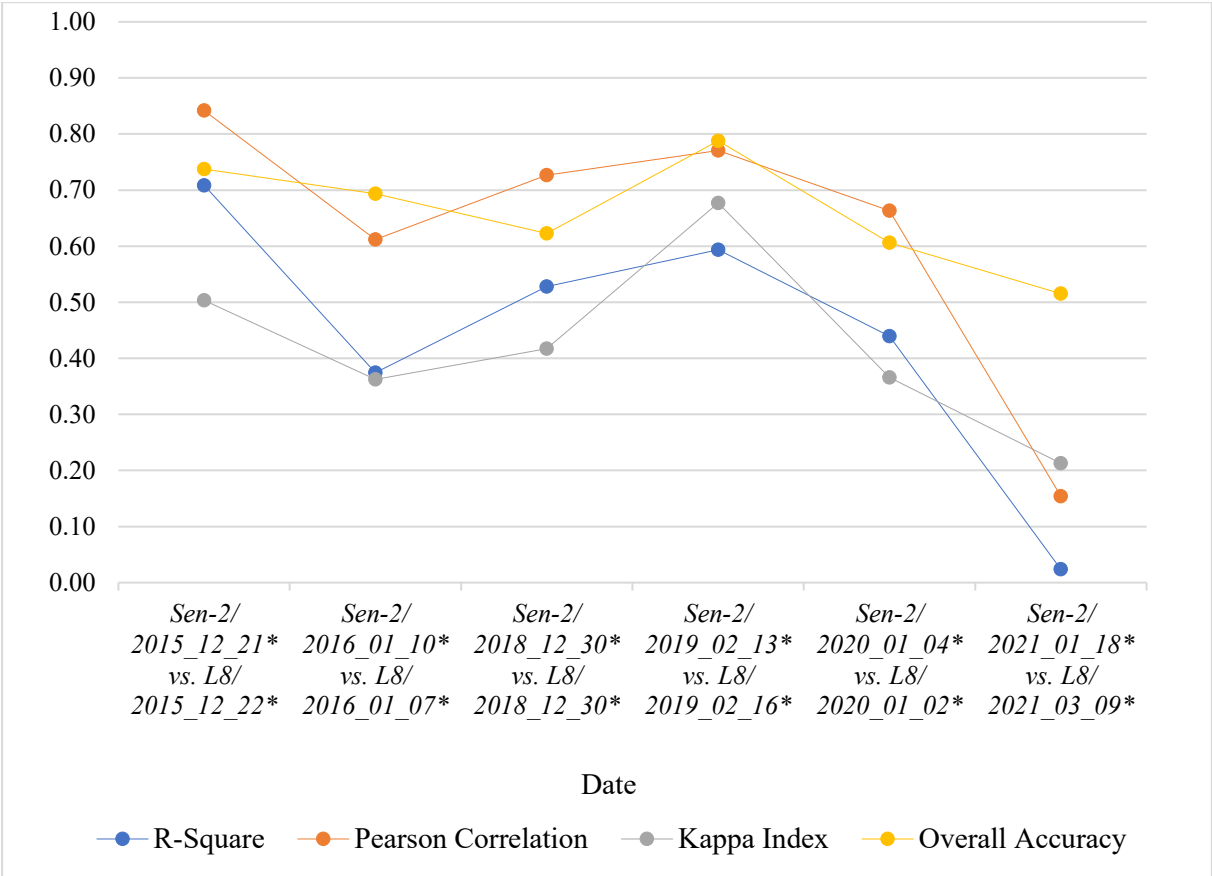

Figure 23. Comparison and correlation coefficients between Sentinel-2 vs. Landsat 8 results.

In Figure 23, it is also interesting to see the results for the date 30.12.2018, which is the only date analyzed that coincides with both satellites revisiting time. On this date, the coefficients behave pretty much as the average values, as well as the spatial classification analysis.
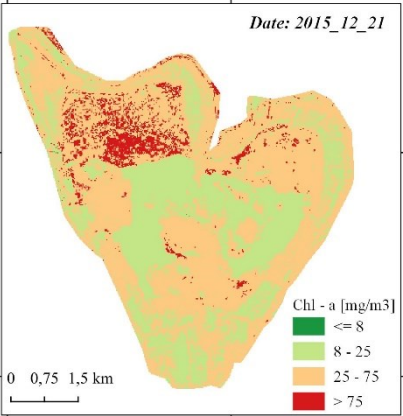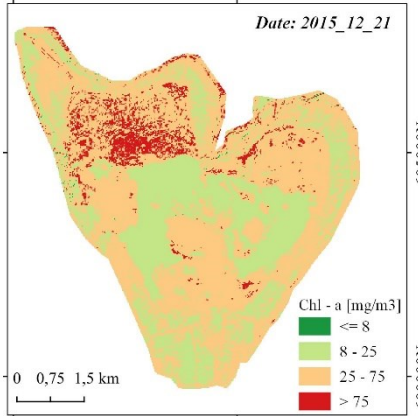
As expected, the worst performance was for the dates in the year 2021, since the data frame was not as close as accurate, due to limited resources in the availability of free cloud imagery for Landsat 8/OLI in January.

3.3.2. Sentinel - 2 with APDA vs. Sentinel-2 DOS

As a complement analysis, two atmospheric correcting methods were evaluated for Sentinel-2 images, the default APDA, obtained with Sen2cor software, and the DOS method obtained with SCP Plugin for QGIS. This, with the aim of seeing the difference in the performance of the algorithm in both atmospheric methods. Results can be seen in Table 7, where the thematic maps present a general pattern of underestimation of Chl-a concentration when using the DOS atmospheric method.

One reason for this could be the scattering effect produced by the compounds found in the atmosphere, which are not as well filtered with the DOS method, since it is an image-based algorithm, while the APDA method relies highly on the water vapor parameter specifically to the region to retrieve an accurate corrected image.
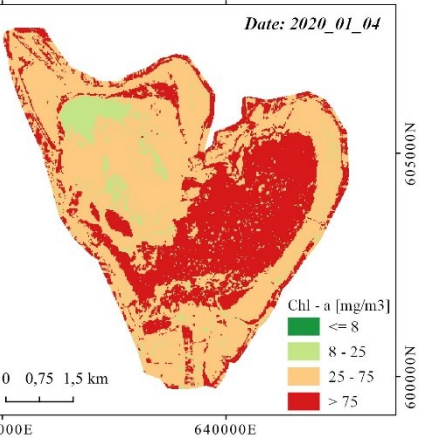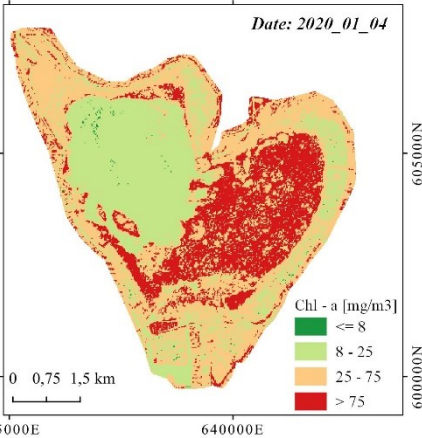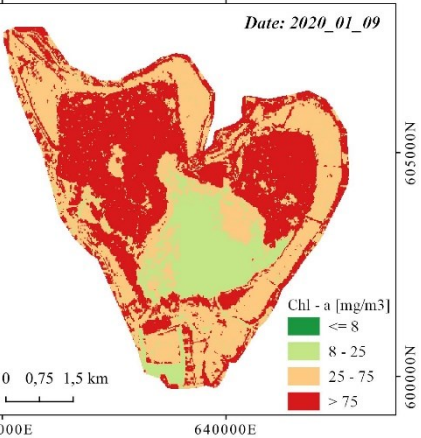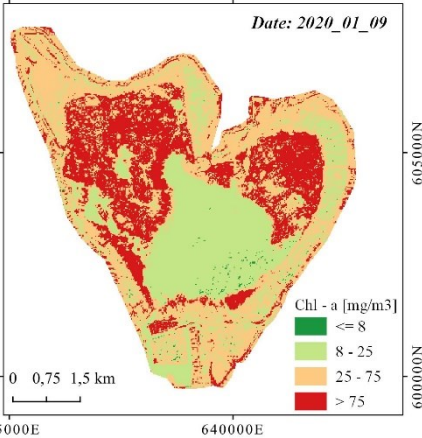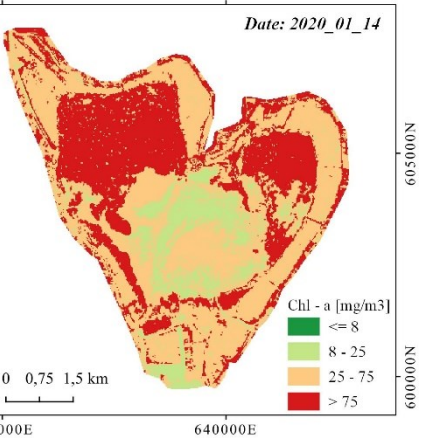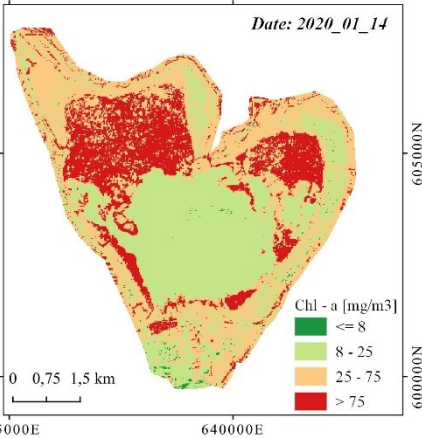
Table 7. *Comparison coefficients between atmospheric correction made by Sen2Cor (with* ***APDA****) and atmospheric correction made by SCP (with* ***DOS*** *algorithm) in Sentinel-2 images for Chl-a estimation.*

Sentinel-2 Corrected with Sen2cor (APDA)	Sentinel-2 Corrected with SCP (DOS)	Coefficients
		RMSE= 5.81 R^2= 0.92 Pearson Correlation= 0.96 Kappa=0.91 O.A=0.94

Sentinel-2 Corrected with Sen2cor (APDA)	Sentinel-2 Corrected with SCP (DOS)	Coefficients
		RMSE= 8.99 R²= 0.84 Pearson Correlation= 0.92 Kappa=0.83 O.A=0.89
		RMSE= 39.02 R²= 0.84 Pearson Correlation= 0.91 Kappa=0.55 O.A=0.69
		RMSE= 38.87 R²= 0.81 Pearson Correlation= 0.90 Kappa=0.24 O.A=0.47

Sentinel-2 Corrected with Sen2cor (APDA)	Sentinel-2 Corrected with SCP (DOS)	Coefficients
Date: 2018_12_25	Date: 2018_12_25	RMSE= 35.44 R²= 0.87 Pearson Correlation= 0.93 Kappa=0.50 O.A=0.66
Date: 2018_12_30	Date: 2018_12_30	RMSE= 41.58 R²= 0.73 Pearson Correlation= 0.85 Kappa=0.37 O.A=57
Date: 2019_01_04	Date: 2019_01_04	RMSE= 32.09 R²= 0.81 Pearson Correlation= 0.90 Kappa=0.54 O.A=0.69
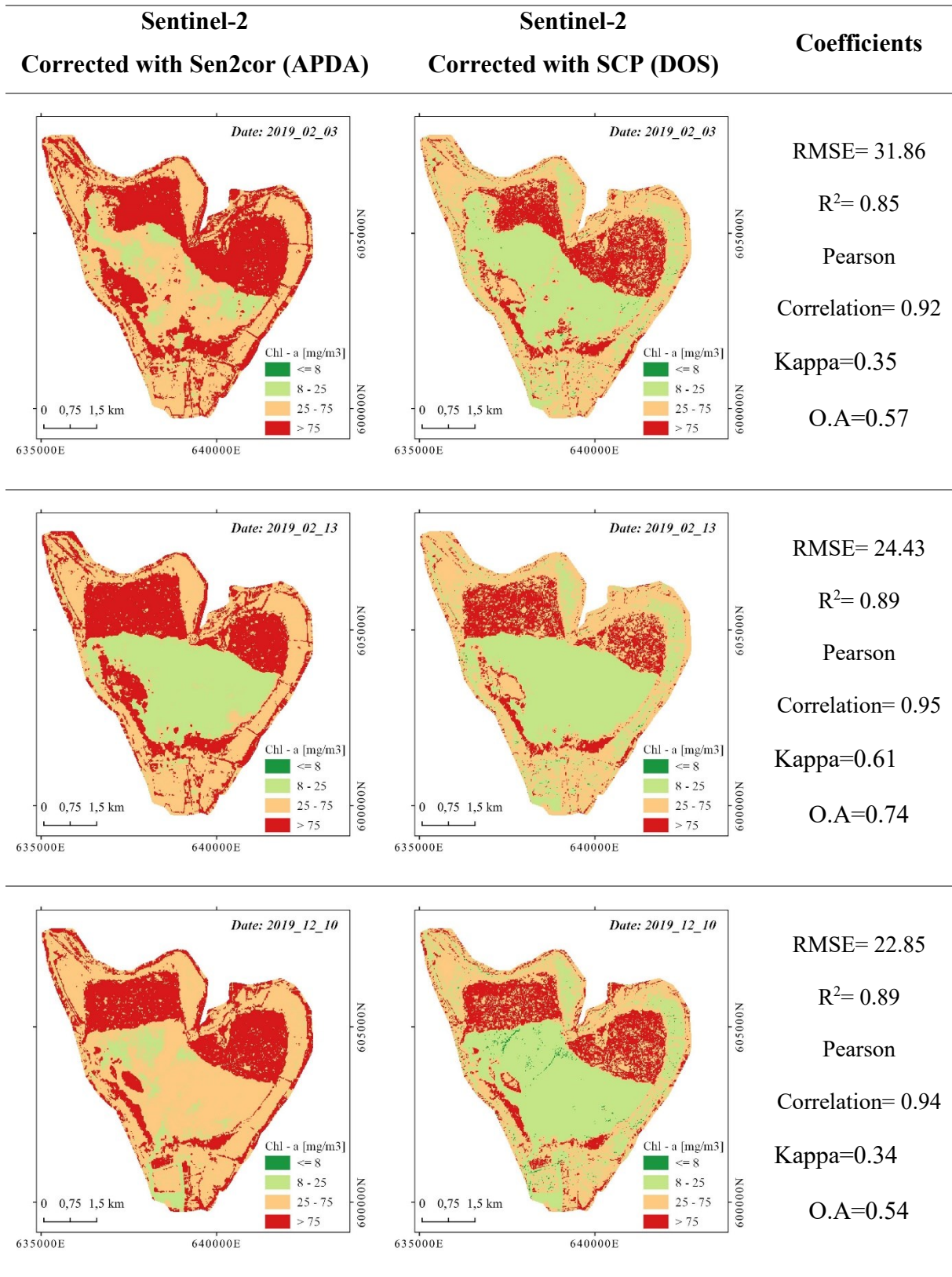
Sentinel-2 Corrected with Sen2cor (APDA)	Sentinel-2 Corrected with SCP (DOS)	Coefficients
		RMSE= 31.86 R^2= 0.85 Pearson Correlation= 0.92 Kappa=0.35 O.A=0.57
		RMSE= 24.43 R^2= 0.89 Pearson Correlation= 0.95 Kappa=0.61 O.A=0.74
		RMSE= 22.85 R^2= 0.89 Pearson Correlation= 0.94 Kappa=0.34 O.A=0.54

Sentinel-2 Corrected with Sen2cor (APDA)	Sentinel-2 Corrected with SCP (DOS)	Coefficients
		RMSE= 21.01 R^2= 0.88 Pearson Correlation= 0.94 Kappa=0.36 O.A=0.57
		RMSE= 33.43 R^2= 0.88 Pearson Correlation= 0.94 Kappa=0.47 O.A=0.66
		RMSE= 29.35 R^2= 0.88 Pearson Correlation= 0.94 Kappa=0.41 O.A=0.60

Sentinel-2 Corrected with Sen2cor (APDA)	Sentinel-2 Corrected with SCP (DOS)	Coefficients
		RMSE= 22.31 R^2= 0.87 Pearson Correlation= 0.93 Kappa=0.61 O.A=0.75
		RMSE= 6.34 R^2= 0.93 Pearson Correlation= 0.96 Kappa=0.84 O.A=0.91
		RMSE= 8.92 R^2= 0.88 Pearson Correlation= 0.94 Kappa=0.73 O.A=0.83

Sentinel-2 Corrected with Sen2cor (APDA)	Sentinel-2 Corrected with SCP (DOS)	Coefficients
		RMSE= 32.12 R^2= 0.86 Pearson Correlation= 0.93 Kappa=0.46 O.A=0.64
		RMSE= 34.45 R^2= 0.85 Pearson Correlation= 0.92 Kappa=0.50 O.A=0.67

*O.A.= Overall Accuracy Index, Kappa= Kappa Index, RMSE= Root Mean Square Error, R^2 = Determination r- square coefficient.

To simplify the visualization of the data, the coefficients obtained can be seen displayed in Figure 24. Here the tendency for the pixel-by-pixel comparison seems to be stable and adequate, with an average determination coefficient R^2 value of 0.86, and an average Pearson correlation matrix value of 0.93, which indicates high reciprocity in the values obtained for Chl-a concentration using both atmospheric correcting methods. However, when analyzing the results of the classification accuracy, coefficients were not as high as expected, in fact, data from the dates 2015_12_21 and 2016_01_10 were discarded since they appear to be atypical data, and, so it would probably affect the result of the computed average, which for the Kappa Index was 0.49, and for the overall accuracy was 0.66.
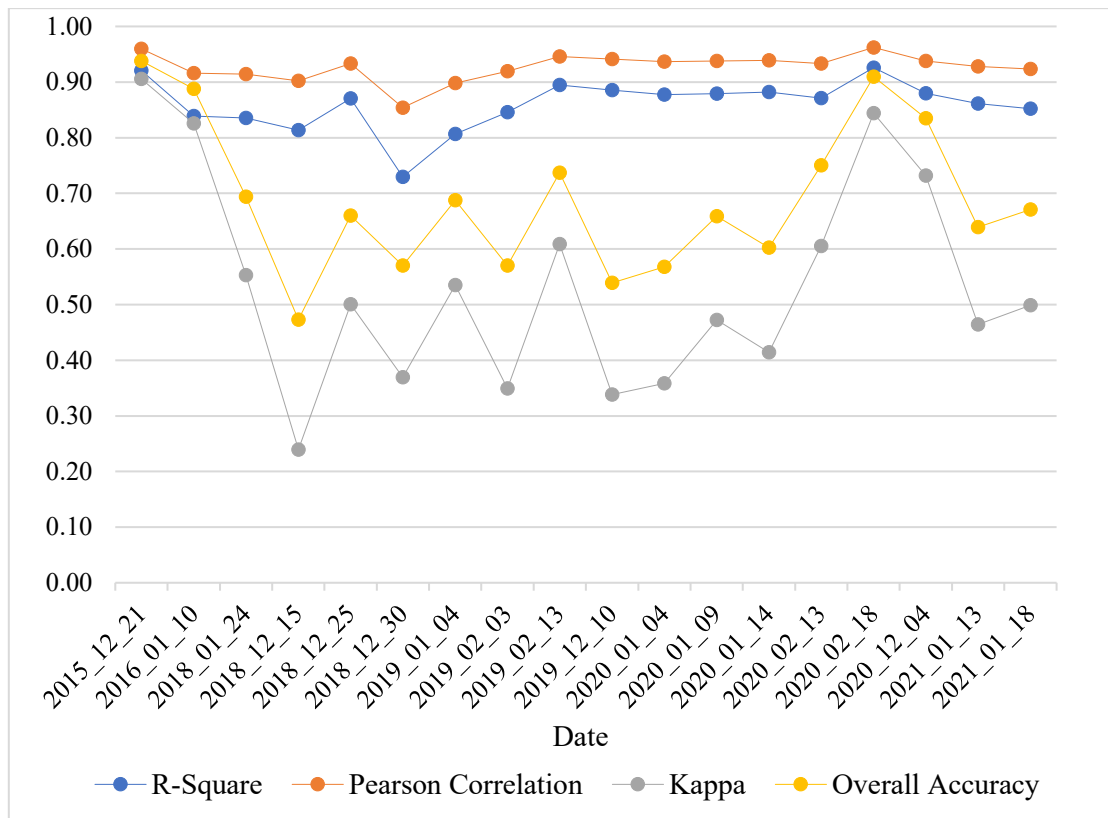
Figure 24. Comparison and correlation coefficients between atmospheric correction methods APDA vs. DOS in Sentinel-2 results.

4. SUMMARY

In this study, the effect of the atmospherical correction methods APDA, DOS, and LaSCR in the potential applicability of Sentinel-2 and Landsat 8 images for estimating Chl a concentration in Fúquene Lagoon was analyzed and compared. To accomplish this, the bottom of the atmosphere reflectance values were computed. In the case of Landsat 8, the imagery was acquired with the LaSRC atmospheric correcting method provided by the USGS, while Sentinel-2 imagery, were processed in the software Sen2cor, using the APDA method. In addition, the DOS method was applied to Sentinel-2 images, to achieve a more complete statistical analysis of the performance and relative applicability of the algorithm.

The Chl-a concentration was estimated using a water quality extraction empirical algorithm, derived from the NDCI and proposed by Page et al. (2018), which has been used and validated by researchers in tropical environments.

The working bands used for the processing of the satellite imagery were band 4 and band 5, for both Sentinel-2 and Landsat 8 (see Table 3), even though there was a limitation for the band 5 in Landsat 8 since the peak wavelength was bigger than the recommended for the Chl-a estimation.

Results provided the spatial distribution of Chl a concentration throughout the year 2015 to the year 2021 during the dry season of Fúquene lagoon, applying the classification threshold methodology proposed by the OECD, in both satellites (Figures 14 to 20). As a general output, there was an overestimation of the Chl-a concentration for Sentinel-2 images when corrected with the APDA method in relation to the results from Landsat 8 and Sentinel-2 images corrected with the DOS method.

Correlation and comparison analysis performed between different sensors, Sentinel -2 and Landsat 8, showed that the methodology followed for Chl-a estimation, could be used in both satellites, having an average Pearson correlation value of 0.77, but the classification method should be improved in order to obtain comparable results in the distribution of Chl-a for both satellites with this algorithm, since the Kappa index reached just a 0.43 value, showing a fault in the classification of the trophic categories.

For the comparison analysis made for Sentinel-2 using different atmospheric correction methods, the APDA, and DOS, the results showed a similar pattern as with the correlation analysis made with Landsat 8. Values for Chl-a concentration were similar with a Pearson

correlation value of 0.93. But, the classification of the categories was not comparable and only reached a Kappa index value of 0.49 and an overall accuracy of 0.66, meaning the classification threshold method could not be applied using the DOS atmospheric correcting method.

The real applicability of the algorithm could not be validated due to the lack of in situ measurements for Chl-a parameter in the Fúquene lagoon, so to make a statistical comparison, Sentinel-2 images, corrected with the APDA method, were selected to work as reference or base-line to compare the other options because they have the wavelength band recommended for Chl-a estimation, as well as the most accurate atmospheric correction method.

This research confirms the need for further validation analysis between the sensor images and the in situ data for the Fúquene lagoon in order to enhance or decreased discrepancies resulting from the atmospherical correction methods and to improve the performance in estimating Chl-a concentrations using water quality algorithms.

Furthermore, the need for improved bio-optical algorithms is confirmed for this study region, since there was not literature covering this topic for Colombian lakes and the algorithm used was selected due to a previous case in Brazilian inland waters. Nevertheless, according to the obtained findings, there is potential applicability of the Sentinel-2 and Landsat 8 imagery as valuable data sources for mapping Chl – a concentrations in Fúquene lagoon, and possibly other Colombian lakes.

REFERENCES

Bukata, R. P., Jerome, J. H., Kondratyev, A. S., & Pozdnyakov, D. V. (2018). *Optical Properties and Remote Sensing of Inland and Coastal Waters*. CRC Press. https://books.google.hu/books?id=aksPEAAAQBAJ

Buma, W. G., & Lee, S.-I. (2020). Evaluation of Sentinel-2 and Landsat 8 Images for Estimating Chlorophyll-a Concentrations in Lake Chad, Africa. *Remote Sensing*, *12*(15), 2437. https://doi.org/10.3390/rs12152437

Campbell, J. B., & Wynne, R. H. (2011). *Introduction to Remote Sensing, Fifth Edition*. Guilford Publications. https://books.google.hu/books?id=NkLmDjSS8TsC

CAR. (2018). *Plan de Manejo Ambiental Distrito Regional de Manejo Integrado para el Complejo Lagunar Fúquene, Cucunubá y Palacio.* (p. 634) [Environmental Assesment Plan]. CAR.

Castillo, I. M., & Rodríguez, M. Á. (2017). Dinámica multitemporal de las coberturas y el espejo de agua en la laguna de Fúquene. *Revista Mutis*, *7*(1), 20–33. https://doi.org/10.21789/22561498.1183

Chavez, J., Pat. (1996). Image-Based Atmospheric Corrections—Revisited and Improved. *Photogrammetric Engineering and Remote Sensing*, *62*, 1025–1036.

Chuvieco, E., & Huete, A. (2009). *Fundamentals of Satellite Remote Sensing*. CRC Press. https://books.google.hu/books?id=tna9CgAAQBAJ

Dong, P., & Chen, Q. (2017). *LiDAR Remote Sensing and Applications*. CRC Press. https://books.google.hu/books?id=utZCDwAAQBAJ

Doxani, G., Vermote, E., Roger, J.-C., Gascon, F., Adriaensen, S., Frantz, D., Hagolle, O., Hollstein, A., Kirches, G., Li, F., Louis, J., Mangin, A., Pahlevan, N., Pflug, B., & Vanhellemont, Q. (2018). Atmospheric Correction Inter-Comparison Exercise. *Remote Sensing*, *10*(3), 352. https://doi.org/10.3390/rs10020352

Duan, H., Ma, R., Xu, J., Zhang, Y., & Zhang, B. (2010). Comparison of different semi-empirical algorithms to estimate chlorophyll-a concentration in inland lake water. *Environmental Monitoring and Assessment*, *170*(1–4), 231–244. https://doi.org/10.1007/s10661-009-1228-7

ESA. (2020a). *Radiometric Resolutions Sentinel-2 MSI User Guides Sentinel Online* [Governmental]. https://sentinels.copernicus.eu/web/sentinel/user-guides/sentinel-2-msi/resolutions/radiometric

ESA. (2020b). *SNAP Supported Plugins Sen2Cor* [Governmental]. ESA. https://step.esa.int/main/snap-supported-plugins/sen2cor/

Estruch, F. (2010). *Análisis de la clorofila a en el agua a partir de una imagen multiespectral Quickbird en la zona costera de Gandia.* [Universidad Politecnica de Valencia]. https://riunet.upv.es/bitstream/handle/10251/9176/Proyecto%20Final%20de%20Carre ra%20-%20Clorofila%20a%20Quickbird.pdf

Gitelson, A. A., Dall'Olmo, G., Moses, W., Rundquist, D. C., Barrow, T., Fisher, T. R., Gurlin, D., & Holz, J. (2008). A simple semi-analytical model for remote estimation of chlorophyll-a in turbid waters: Validation. *Remote Sensing of Environment*, *112*(9), 3582–3593. https://doi.org/10.1016/j.rse.2008.04.015

Global Nature Fund. (2011). *Living Lakes America*. Global Nature. https://www.globalnature.org/en/laguna-fuquene

Gurlin, D., Gitelson, A. A., & Moses, W. J. (2011). Remote estimation of chl-a concentration in turbid productive waters, Return to a simple two-band NIR-red model? *Remote Sensing of Environment*, *115*(12), 3479–3490. https://doi.org/10.1016/j.rse.2011.08.011

Ha, N. T. T., Thao, N. T. P., Koike, K., & Nhuan, M. T. (2017). Selecting the Best Band Ratio to Estimate Chlorophyll-a Concentration in a Tropical Freshwater Lake Using Sentinel 2A Images from a Case Study of Lake Ba Be (Northern Vietnam). *ISPRS International Journal of Geo-Information*, *6*(9), 290. https://doi.org/10.3390/ijgi6090290

IOCCG. (2000). *Remote sensing of ocean color in coastal, and other optically-complex, waters.* [140pp.]. https://doi.org/10.25607/OBP-95

Jenkerson, C. (2020). *Landsat 8 Collection 2 (C2) Level 2 Science Product (L2SP) Guide*. 43.

Jerlov, N. G. (2014). *Optical Oceanography*. Elsevier Science. https://books.google.hu/books?id=k9EjXyVJH0UC

Lima, T. A., Beuchle, R., Langner, A., Grecchi, R. C., Griess, V. C., & Achard, F. (2019). Comparing Sentinel-2 MSI and Landsat 8 OLI Imagery for Monitoring Selective

Logging in the Brazilian Amazon. *Remote Sensing*, *11*(8), 961. https://doi.org/10.3390/rs11080961

Louis, J., Debaecker, V., Pflug, B., Main-Knorn, M., Bieniarz, J., Mueller-Wilm, U., Cadau, E., & Gascon, F. (2016). *SENTINEL-2 SEN2COR: L2A PROCESSOR FOR USERS*. 8.

Mishra, D. R., Ogashawara, I., & Gitelson, A. A. (2017). *Bio-optical Modeling and Remote Sensing of Inland Waters*. Elsevier Science. https://books.google.hu/books?id=jgNQCwAAQBAJ

Mishra, S., & Mishra, D. R. (2012). Normalized difference chlorophyll index: A novel model for remote estimation of chlorophyll-a concentration in turbid productive waters. *Remote Sensing of Environment*, *117*, 394–406. https://doi.org/10.1016/j.rse.2011.10.016

Morel, A., & Prieur, L. (1977). Analysis of variations in ocean color1: Ocean color analysis. *Limnology and Oceanography*, *22*(4), 709–722. https://doi.org/10.4319/lo.1977.22.4.0709

OECD. (1982). OECD: Eutrophication of Waters. Monitoring, Assessment and Control. — 154 pp. Paris: Organisation for Economic Co-Operation and Development 1982. (Publié en français sous le titre »Eutrophication des Eaux. Méthodes de Surveillance, d'Evaluation et de Lutte«). *Internationale Revue der gesamten Hydrobiologie und Hydrographie*, *69*(2), 200–200. https://doi.org/10.1002/iroh.19840690206

Page, B. P., Kumar, A., & Mishra, D. R. (2018). A novel cross-satellite-based assessment of the Spatio-temporal development of a cyanobacterial harmful algal bloom. *International Journal of Applied Earth Observation and Geoinformation*, *66*, 69–81. https://doi.org/10.1016/j.jag.2017.11.003

Page, B. P., Olmanson, L. G., & Mishra, D. R. (2019). A harmonized image processing workflow using Sentinel-2/MSI and Landsat-8/OLI for mapping water clarity in optically variable lake systems. *Remote Sensing of Environment*, *231*, 111284. https://doi.org/10.1016/j.rse.2019.111284

Pahlevan, N., Lee, Z., Wei, J., Schaaf, C. B., Schott, J. R., & Berk, A. (2014). On-orbit radiometric characterization of OLI (Landsat-8) for applications in aquatic remote sensing. *Remote Sensing of Environment*, *154*, 272–284. https://doi.org/10.1016/j.rse.2014.08.001

Pereira, A. R. A., Lopes, J. B., Espindola, G. M. de, Silva, C. E. da, Pereira, A. R. A., Lopes, J. B., Espindola, G. M. de, & Silva, C. E. da. (2020). Retrieval and mapping of chlorophyll-a concentration from Sentinel-2 images in an urban river in the semiarid region of Brazil. *Revista Ambiente & Água*, *15*(2). https://doi.org/10.4136/ambi-agua.2488

Preisendorfer, R. W., Laboratory (U.S.), P. M. E., & Laboratories (U.S.), E. R. (1976). *Hydrologic Optics*. U.S. Department of Commerce, National Oceanic and Atmospheric Administration, Environmental Research Laboratories, Pacific Marine Environmental Laboratory. https://books.google.hu/books?id=-4CrJo8gp8YC

Sabins, F. F. (2007). *Remote Sensing: Principles and Applications, Third Edition*. Waveland Press. https://books.google.hu/books?id=nVgfAAAAQBAJ

Sabins, F. F., & Ellis, J. M. (2020). *Remote Sensing: Principles, Interpretation, and Applications, Fourth Edition*. Waveland Press. https://books.google.hu/books?id=rAnaDwAAQBAJ

Topp, S. N., Pavelsky, T. M., Jensen, D., Simard, M., & Ross, M. R. V. (2020a). *Research Trends in the Use of Remote Sensing for Inland Water Quality Science: Moving Towards Multidisciplinary Applications*. 34.

Topp, S. N., Pavelsky, T. M., Jensen, D., Simard, M., & Ross, M. R. V. (2020b). Research Trends in the Use of Remote Sensing for Inland Water Quality Science: Moving Towards Multidisciplinary Applications. *Water*, *12*(1), 169. https://doi.org/10.3390/w12010169

Tyler, A. N., Hunter, P. D., Spyrakos, E., Groom, S., Constantinescu, A. M., & Kitchen, J. (2016). Developments in Earth observation for the assessment and monitoring of inland, transitional, coastal and shelf-sea waters. *Science of The Total Environment*, *572*, 1307–1321. https://doi.org/10.1016/j.scitotenv.2016.01.020

USGS. (n.d.). *Landsat missions: Landsat 8* [Governmental]. USGS. Retrieved April 5, 2021, from https://www.usgs.gov/core-science-systems/nli/landsat/landsat-8?qt-science_support_page_related_con=0#qt-science_support_page_related_con

USGS. (2018). *What are the band designations for the Landsat satellites?* (Fact Sheet) [Fact Sheet].

VectorMine. (n.d.). *Remote sensing vector illustration. Satellite data wave acquisition scheme.* VectorMine. Retrieved March 7, 2021, from https://vectormine.com/item/6044d7d051b32614b4cfe752

Watanabe, F., Alcântara, E., Rodrigues, T., Rotta, L., Bernardo, N., & Imai, N. (2018). Remote sensing of the chlorophyll-a based on OLI/Landsat-8 and MSI/Sentinel-2A (Barra Bonita reservoir, Brazil). *Anais Da Academia Brasileira de Ciências*, *90*(2 suppl 1), 1987–2000. https://doi.org/10.1590/0001-3765201720170125

Yigit Avdan, Z., Kaplan, G., Goncu, S., & Avdan, U. (2019). Monitoring the Water Quality of Small Water Bodies Using High-Resolution Remote Sensing Data. *ISPRS International Journal of Geo-Information*, *8*(12), 553. https://doi.org/10.3390/ijgi8120553
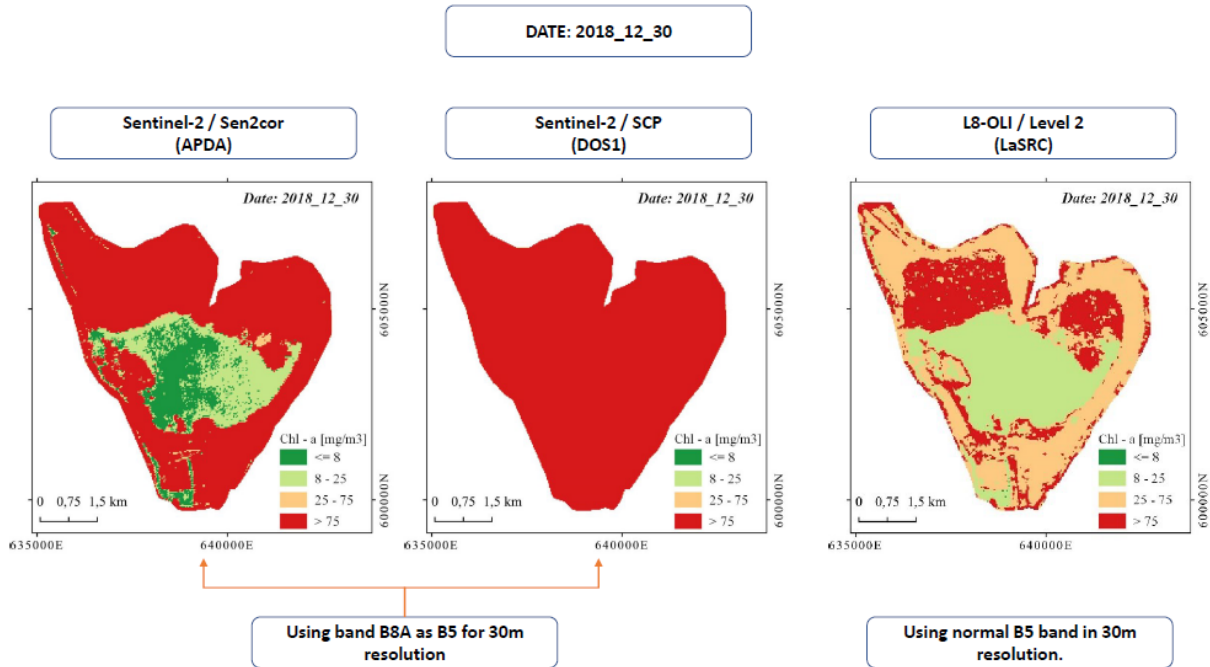
ANNEX

Annex 1. Compiled results statistics of the rasters for estimation of Chl-a in Fuquene Lagoon.

Image		Chl-a raster statistics (mg/m3)				Oligotrophic < 8 (mg/m3)			Mesotrophic 8 -25 (mg/m3)			Eutrophic 25 - 75 (mg/m3)			Hypertrophic >75 (mg/m3)		
Satellite/Sensor	Date	Min.	Mean	Max.	STD	Pixel count	Area (Km²)	Area (Ha)	Pixel count	Area (Km²)	Area (Ha)	Pixel count	Area (Km²)	Area (Ha)	Pixel count	Area (Km²)	Area (Ha)
Sentinel-2A MSI	2015_12_21	5.84	38.14	106.27	20.23	5.00	0.00	0.45	13293.00	11.96	1196.37	23567.00	21.21	2121.03	2266.00	2.04	203.94
Sentinel-2A MSI	2016_01_10	4.59	44.61	116.44	21.64	7.00	0.01	0.63	9200.00	8.28	828.00	25619.00	23.06	2305.71	4305.00	3.87	387.45
Sentinel-2B MSI	2018_01_24	4.80	78.77	262.92	49.56	4.00	0.00	0.36	10580.00	9.52	952.20	8421.00	7.58	757.89	20126.00	18.11	1811.34
Sentinel-2A MSI	2018_12_15	7.79	77.67	294.48	46.23	2.00	0.00	0.18	918.00	0.83	82.62	21227.00	19.10	1910.43	16984.00	15.29	1528.56
Sentinel-2A MSI	2018_12_25	6.60	75.98	294.48	49.37	3.00	0.00	0.27	6680.00	6.01	601.20	15566.00	14.01	1400.94	16882.00	15.19	1519.38
Sentinel-2B MSI	2018_12_30	6.50	77.25	294.48	49.33	6.00	0.01	0.54	5106.00	4.60	459.54	16819.00	15.14	1513.71	17200.00	15.48	1548.00
Sentinel-2A MSI	2019_01_04	4.68	66.81	228.58	43.10	9.00	0.01	0.81	7417.00	6.68	667.53	17261.00	15.53	1553.49	14444.00	13.00	1299.96
Sentinel-2A MSI	2019_02_03	6.87	71.08	275.98	40.33	2.00	0.00	0.18	3478.00	3.13	313.02	19751.00	17.78	1777.59	15900.00	14.31	1431.00
Sentinel-2A MSI	2019_02_13	10.28	61.19	174.85	37.39	0.00	0.00	0.00	10685.00	9.62	961.65	14777.00	13.30	1329.93	13669.00	12.30	1230.21
Sentinel-2A MSI	2019_12_10	7.62	61.47	168.68	35.57	1.00	0.00	0.09	3052.00	2.75	274.68	22821.00	20.54	2053.89	13257.00	11.93	1193.13
Sentinel-2B MSI	2020_01_04	9.11	63.27	160.71	33.29	0.00	0.00	0.00	2221.00	2.00	199.89	22648.00	20.38	2038.32	14262.00	12.84	1283.58

Image		Chl-a raster statistics (mg/m3)				Oligotrophic < 8 (mg/m3)			Mesotrophic 8 -25 (mg/m3)			Eutrophic 25 - 75 (mg/m3)			Hypertrophic >75 (mg/m3)		
Satellite/Sensor	Date	Min.	Mean	Max.	STD	Pixel count	Area (Km²)	Area (Ha)	Pixel count	Area (Km²)	Area (Ha)	Pixel count	Area (Km²)	Area (Ha)	Pixel count	Area (Km²)	Area (Ha)
Sentinel-2A MSI	2020_01_09	5.03	75.08	236.45	46.16	15.00	0.01	1.35	5767.00	5.19	519.03	15924.00	14.33	1433.16	17425.00	15.68	1568.25
Sentinel-2B MSI	2020_01_14	6.47	66.97	207.76	41.87	2.00	0.00	0.18	4806.00	4.33	432.54	20026.00	18.02	1802.34	14297.00	12.87	1286.73
Sentinel-2B MSI	2020_02_13	9.18	50.96	186.69	35.50	0.00	0.00	0.00	13046.00	11.74	1174.14	17112.00	15.40	1540.08	8973.00	8.08	807.57
Sentinel-2A MSI	2020_02_18	4.56	33.18	110.54	22.94	66.00	0.06	5.94	19605.00	17.64	1764.45	16038.00	14.43	1443.42	3422.00	3.08	307.98
Sentinel-2A MSI	2020_12_04	5.83	44.03	114.39	25.12	11.00	0.01	0.99	12575.00	11.32	1131.75	19747.00	17.77	1777.23	6798.00	6.12	611.82
Sentinel-2A MSI	2021_01_13	4.50	68.26	230.26	45.56	76.00	0.07	6.84	6758.00	6.08	608.22	17274.00	15.55	1554.66	15023.00	13.52	1352.07
Sentinel-2B MSI	2021_01_18	4.50	75.59	228.51	45.50	61.00	0.05	5.49	3983.00	3.58	358.47	17898.00	16.11	1610.82	17189.00	15.47	1547.01
Landsat 8 OLI	2015_01_04	6.18	49.97	124.31	28.09	36.00	0.03	3.24	9820.00	8.84	883.80	19864.00	17.88	1787.76	9411.00	8.47	846.99
Landsat 8 OLI	2015_12_22*	8.46	47.14	126.36	24.62	0.00	0.00	0.00	7866.00	7.08	707.94	25248.00	22.72	2272.32	6017.00	5.42	541.53
Landsat 8 OLI	2016_01_07*	8.45	46.38	119.55	22.71	0.00	0.00	0.00	7101.00	6.39	639.09	27037.00	24.33	2433.33	4993.00	4.49	449.37
Landsat 8 OLI	2016_01_23	9.72	45.07	115.42	20.78	0.00	0.00	0.00	6506.00	5.86	585.54	29044.00	26.14	2613.96	3581.00	3.22	322.29
Landsat 8 OLI	2016_11_22	6.30	47.91	123.31	24.73	8.00	0.01	0.72	9341.00	8.41	840.69	23522.00	21.17	2116.98	6260.00	5.63	563.40
Landsat 8 OLI	2018_12_30*	5.56	50.67	119.29	30.79	11.00	0.01	0.99	11124.00	10.01	1001.16	16873.00	15.19	1518.57	11123.00	10.01	1001.07
Landsat 8 OLI	2019_02_16*	8.00	47.00	111.03	28.25	0.00	0.00	0.00	11509.00	10.36	1035.81	18491.00	16.64	1664.19	9131.00	8.22	821.79

Image		Chl-a raster statistics (mg/m3)				Oligotrophic < 8 (mg/m3)			Mesotrophic 8 -25 (mg/m3)			Eutrophic 25 - 75 (mg/m3)			Hypertrophic >75 (mg/m3)		
Satellite/Sensor	Date	Min.	Mean	Max.	STD	Pixel count	Area (Km²)	Area (Ha)	Pixel count	Area (Km²)	Area (Ha)	Pixel count	Area (Km²)	Area (Ha)	Pixel count	Area (Km²)	Area (Ha)
Landsat 8 OLI	2019_12_17	12.86	47.36	109.53	26.52	0.00	0.00	0.00	12399.00	11.16	1115.91	18102.00	16.29	1629.18	8630.00	7.77	776.70
Landsat 8 OLI	2020_01_02*	7.83	52.29	123.04	33.41	1.00	0.00	0.09	11145.00	10.03	1003.05	15509.00	13.96	1395.81	12476.00	11.23	1122.84
Landsat 8 OLI	2021_03_09*	6.45	51.27	117.28	28.58	95.00	0.09	8.55	8568.00	7.71	771.12	19334.00	17.40	1740.06	11134.00	10.02	1002.06

Annex 2. Trial using band 8A in Sentinel-2 image with APDA and DOS vs. Landsat 8 with LaSCR.

Annex 3. Scatter plots between Sentinel-2 and Landsat 8 results.

The following figures display the scatter plots for correlational purposes between the Sentinel – 2 and Landsat 8 imagery processed for the concentration of Chlorophyll-a in the Fúquene lagoon.
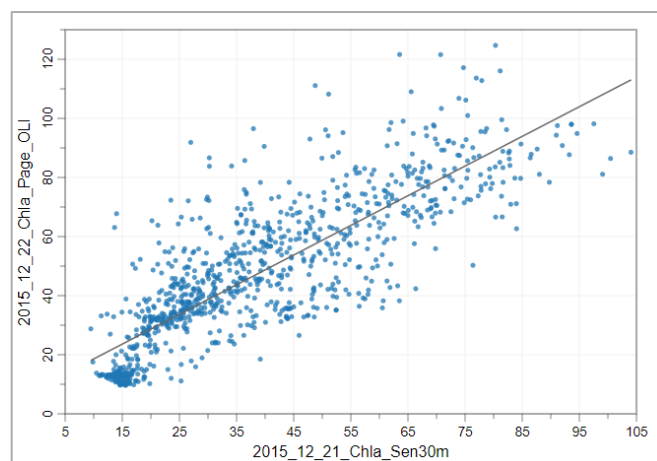

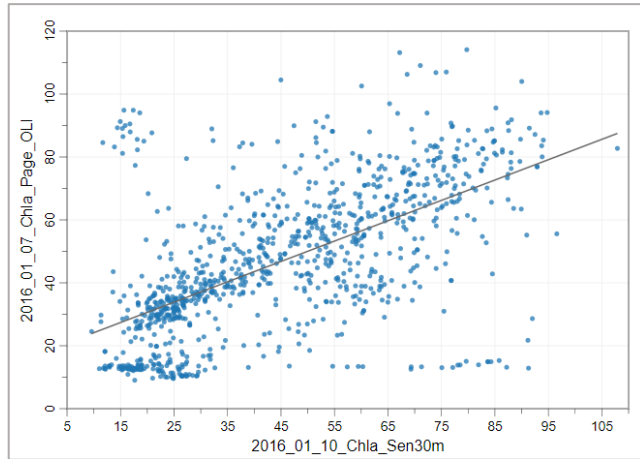*Fig. A 1. Scatter plot between Sen2 2015_12_21 vs. Land8 2015_12_22.*

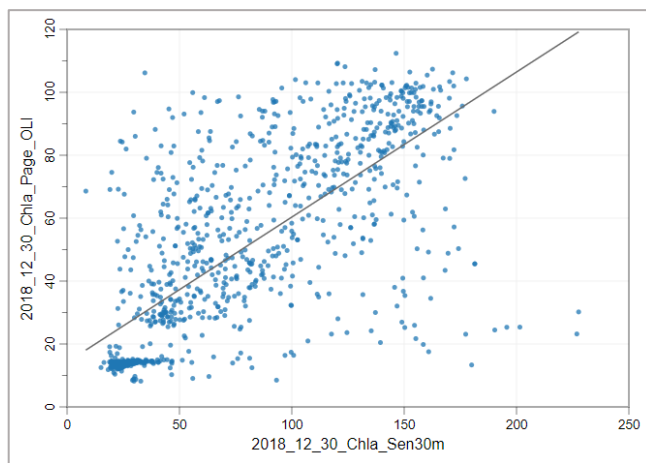*Fig. A 2. Scatter plot between Sen2 2016_01_10 vs. Land8 2016_01_07*

Fig. A 3. Scatter plot between Sen2 2018_12_301 vs. Land8 2018_12_30
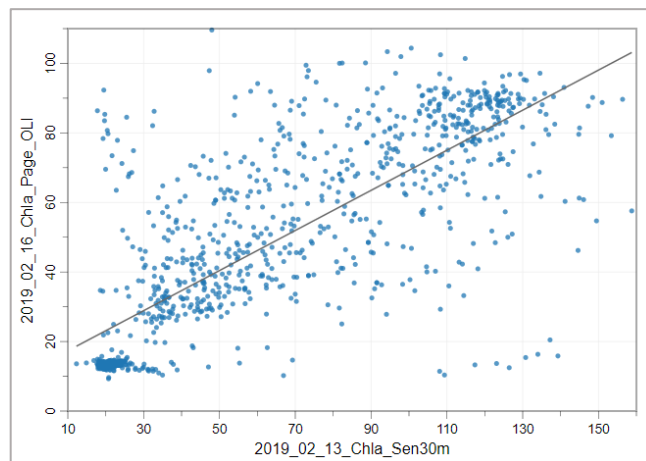

Fig. A 4. Scatter plot between Sen2 2019_02_13 vs. Land8 2019_02_16

Fig. A 5. Scatter plot between Sen2 2020_01_04 vs. Land8 2020_01_02
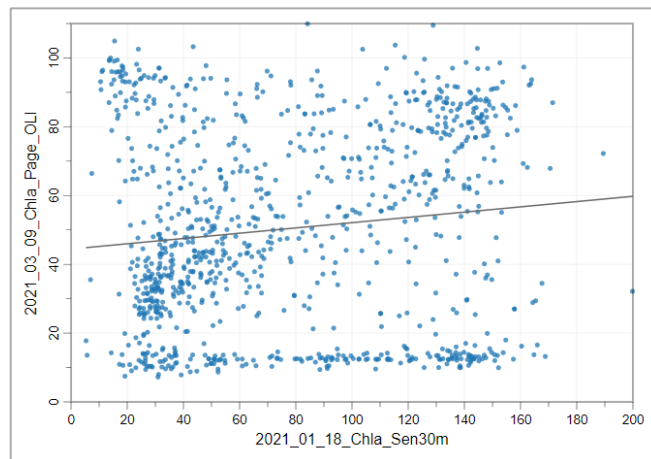

Fig. A 6. Scatter plot between Sen2 2021_01_18 vs. Land8 2021_03_09

DECLARATION

I, undersigned *SARA ALEJANDRA MENDOZA URREA* (NEPTUN CODE: *D07ENT*), declare that the present master's thesis is my original intellectual product in full and that I have not submitted any part or the whole of this work to any other institution. Permissions related to the use of copyrighted sources in this work are attached.

I AGREE to the publication of the accepted master's thesis in pdf form on the website of the Department of Cartography and Geoinformatics.

Budapest, *15 of May of 2021*

_____

(signature of the student)